



Magma-driven accommodation structures formed during sill emplacement at shallow crustal depths: The Maiden Creek sill, Henry Mountains, Utah

Penelope I.R. Wilson¹, Ken J.W. McCaffrey², and Robert E. Holdsworth²

¹Department of Geography and Geology, Kingston University London, Kingston upon Thames KT1 2EE, UK

²Department of Earth Sciences, Durham University, Durham DH13LE, UK

ABSTRACT

In areas of exceptional exposure, upper-crustal intrusions and their immediate wall rocks commonly preserve direct evidence of the emplacement, magma flow pathways, and strains associated with the intrusion process. Such excellent exposure is displayed by the Paleogene Maiden Creek intrusion—a small satellite body related to the Mount Hillers intrusive complex, Henry Mountains, Utah. An intermediate plagioclase-hornblende porphyritic magma was intruded into the Entrada Sandstone Formation at an estimated depth of ~3 km. The southern part of the intrusion is overlain by the newly identified Maiden Creek shear zone (MCSZ): a subhorizontal, top-to-the-WNW detachment formed at the contact with the overlying sandstone country rocks. From observations of both syn-emplacement deformation and the exposed intrusion geometries, it is proposed that the southern Maiden Creek intrusion comprises westerly derived, inclined sill sheets. Host-rock sandstones were sandwiched (~E–W constriction) between these intrusive bodies beneath the MCSZ. It is proposed that the MCSZ is a syn-emplacement magma-driven accommodation structure, with a shear sense antithetic to the magma flow direction, which played a critical role in accommodating the westerly derived sill intrusion. Our results show that inelastic syn-emplacement deformation structures, such as the MCSZ, are very important in the accommodation of magma in the subsurface. Such small structures are unlikely to be imaged by seismic-reflection surveys, highlighting the importance of detailed field studies in our understanding of intrusion geometry and emplacement mechanisms.

1. INTRODUCTION

Large volumes of igneous rock are known to occur in the shallow upper crust (upper 10 km) as intrusive bodies, ranging both in size and geometry (e.g., Cruden and McCaffrey, 2001; Cruden et al., 2018). Our understanding of the 3D geometry and 4D emplacement of igneous intrusions has advanced in recent years through improvements in seismic imaging (e.g., Malthe-Sørensen et al., 2004; Thomson and Schofield, 2008; Magee et al., 2014) and experimental modeling (e.g., Kavanagh et al., 2006, 2015; Galland et al., 2009, 2015; Haug et

al., 2017). However, due to limitations with spatial resolution and appropriate rheological modeling materials, respectively, host-rock structures are generally poorly imaged. Furthermore, over the past few years, there has been a growing sense that magma emplacement cannot wholly be assumed to be an elastic process (e.g., accommodation by elastic bending; Schofield et al., 2012; Haug et al., 2017; Schmiedel et al., 2017; Cruden et al., 2018). Field studies can provide insights into subseismic-scale deformation and also emplacement processes in natural materials. The incorporation of field observations is therefore a key source of evidence to be used in the debate on the mechanics of igneous emplacement in the shallow crust. To date, most field-based studies of intrusions have focused on the geometry and internal architecture of sills, laccoliths, and plutons, using a variety of methods including: field mapping of internal contacts and external margins (e.g., Morgan et al., 2008; Magee et al., 2012; Wilson et al., 2016); geochronological studies (e.g., Coleman et al., 2004; Westerman et al., 2004); magnetic and macroscopic fabric studies (e.g., de Saint Blanquat and Tikoff, 1997; Horsman et al., 2005; Stevenson et al., 2007); and integration of field and numerical modeling (e.g., Pollard and Johnson, 1973). The problem we address here is that few studies have paid close attention to the accommodation structures that form in the host rocks in direct response to intrusion (e.g., Johnson and Pollard, 1973; Jackson and Pollard, 1988; Spacapan et al., 2016; Wilson et al., 2016). The geometry, kinematics, displacement (strain field), and deformation mechanisms displayed by these accommodation structures must be compatible with the intrusion mechanism and magma flow directions, but rarely are these structures discussed or considered in any great detail.

Three distinct and different types of accommodation structures are associated with intrusion emplacement. Preexisting structures that are utilized and/or reactivated during magma emplacement (e.g., Hutton and McErlan, 1991; Holdsworth et al., 1999; Magee et al., 2013) are here termed “pre-emplacement” accommodation structures. The second type comprises large, tectonically driven structures (such as transtensional faults and/or shear zones) that form synchronously with magma emplacement, i.e., “syntectonic” accommodation structures (e.g., Hutton et al., 1990; McCaffrey, 1992; Neves et al., 1996; Passchier et al., 2005). The third type consists of localized structures that develop directly in response to magma intrusion to accommodate the extra volume of

rock either laterally or vertically within the host rocks; in this case, deformation is driven purely by magma emplacement (e.g., Johnson and Pollard, 1973; Spacapan et al., 2016; Wilson et al., 2016). It is this final group of understudied “syn-emplacement” accommodation structures and associated physical mechanisms that are the most informative with regard to emplacement mechanism and are the principal focus of this study.

The present field-based study focuses on a previously undocumented, syn-emplacement accommodation structure—the Maiden Creek shear zone (MCSZ), which we argue was formed solely during emplacement of the late Paleogene Maiden Creek intrusion in the Henry Mountains, Utah (Fig. 1). The study combines traditional field mapping and structural studies, microstructural analysis, and 3D visualization to provide a detailed analysis of the geometries, kinematics, and spatial distribution of the MCSZ in both the intrusion and host rocks. We discuss the MCSZ and show how understanding its role as a syn-emplacement accommodation structure leads to a significant reinterpretation of the emplacement mechanism for parts of the Maiden Creek intrusion.

2. GEOLOGICAL SETTING

2.1. Henry Mountains

The Henry Mountains, southeast Utah, form part of the Colorado Plateau (Fig. 1A) and are a classic region for the study of shallow-level igneous intrusions and their emplacement. Following the ground-breaking research of Gilbert in the late nineteenth century (Gilbert, 1877, 1896), a variety of studies have been carried out in the range (e.g., Hunt, 1953; Johnson and Pollard, 1973; Jackson and Pollard, 1988; Nelson and Davidson, 1993; Habert and de Saint Blanquat, 2004; Horsman et al., 2005; de Saint-Blanquat et al., 2006; Morgan et al., 2008; Wetmore et al., 2009; Wilson and McCaffrey, 2013; Wilson et al., 2016). Five principal peaks (from north to south: Mount Ellen, Mount Pennell, Mount Hillers, Mount Holmes, and Mount Ellsworth) make up the Henry Mountains, each peak corresponding to an intrusive center (Fig. 1A). The igneous rocks are late Paleogene in age (Oligocene, 31.2–23.3 Ma, K-Ar ages; Nelson et al., 1992), and most are of an intermediate, dioritic composition (58%–63% SiO₂; Hunt, 1953; Engel, 1959; Nelson et al., 1992). They have a porphyritic texture, with dominant plagioclase (An²⁰ to An⁶⁰; 20%–40%) and hornblende (5%–15%) phenocrysts (Nelson et al., 1992). Although broadly consistent in composition, the porphyritic textural characteristics vary significantly from one intrusion to another (Hunt, 1953; Nelson et al., 1992).

The intrusions were emplaced into a 3–6-km-thick section of late Paleozoic–Mesozoic sedimentary rocks overlying Precambrian crystalline basement (Jackson and Pollard, 1988; Hintze and Kowallis, 2009) and postdate minor Laramide orogenic activity (Late Cretaceous to early Paleogene in age; Davis, 1978; Davis, 1999) in the Colorado Plateau. Although Laramide structures are present locally (Davis, 1978; Jackson and Pollard, 1988; Bump and Davis, 2003), the strata into which the Henry Mountains intrusions are emplaced are nearly

flat lying (Jackson and Pollard, 1988). Lack of significant pre- and post-emplacement tectonism aids the preservation of both intrusion geometries and emplacement-related deformation structures.

2.2. Maiden Creek Intrusion

A number of small satellite intrusions flank the north and northeast margins of Mount Hillers (Fig. 1A). Due to the excellent exposure giving access to 3D intrusion geometries, a number of these intrusions have been studied in detail and are considered to be classic examples of sill and laccolith intrusions (e.g., Gilbert, 1877; Hunt, 1953; Johnson and Pollard, 1973; Habert and de Saint Blanquat, 2004; Horsman et al., 2005; de Saint-Blanquat et al., 2006; Morgan et al., 2008; Horsman et al., 2009; Wilson et al., 2016). The Maiden Creek body forms one of the most distal satellite intrusions of the Mount Hillers complex, lying ~10 km NE from the main intrusive center (Fig. 1A). Neighboring satellite bodies include the Sawtooth Ridge, the Black Mesa bysmalith, and the Trachyte Mesa intrusions.

The Maiden Creek body is a small (~1 km² in map view; Fig. 1B), sub-horizontal intrusion and has been referred to as a sill in previous studies (e.g., Hunt, 1953; Johnson and Pollard, 1973; Horsman et al., 2005, 2009). It intrudes, and is concordant with, the Entrada Sandstone Formation of the Jurassic San Rafael Group (Gilbert, 1877; Hunt, 1953; Johnson and Pollard, 1973; Horsman et al., 2005). From the abundance of lateral contacts between the intrusion and its host rocks, Horsman et al. (2005) proposed that it is formed by a main sill-like body (with a tabular geometry in 3D and elliptical in map view) with four protruding, finger-like lobes: a pair of lobes trending roughly NE–SW in the northeast and a second pair trending ~N–S to the south (Fig. 1B). Horsman et al. (2005, 2009) discussed evidence for two vertically stacked bulbous terminations along the intrusion margins and highlighted a narrow band of solid-state fabrics within the intrusion. On this basis, they suggested that the intrusion consists of two vertically stacked igneous sheets, with the later sheet intruded above the first (i.e., an example of over accretion; Menand, 2008) and with an almost identical thickness and extent to the first. The southern pair of intrusive lobes forms the focus of the present paper (Figs. 1C and 1D; Supplemental Materials 1¹) due to the excellent exposures of intrusion–host-rock contacts and abundance of syn-emplacement accommodation structures (Fig. 2).

Petrographic analyses show that away from regions of deformation close to the margins, the intrusion has a porphyritic texture dominated by subhedral- to euhedral-zoned plagioclase laths (≤10 mm in size with an average of ~3 mm) and hornblende needles (≤5 mm in length) set within a fine-grained matrix with similar mineralogy to that of the phenocrysts (Figs. 3A and 3B). The sample shown in Figures 3A and 3B exhibits textures typically seen over much of the intrusion; internal deformation appears to be minimal, with euhedral phenocrysts preserving crystallization textures (e.g., twinning and pseudo-oscillatory zoning in the plagioclases and cleavage in the hornblendes; Fig. 3B).



¹Supplemental Materials 1. Google Earth™ project (.kmz file) with locations of structural stations. Please visit <https://doi.org/10.1130/GES02067.S1> or access the full-text article on www.gsapubs.org to view Supplemental Materials 1.

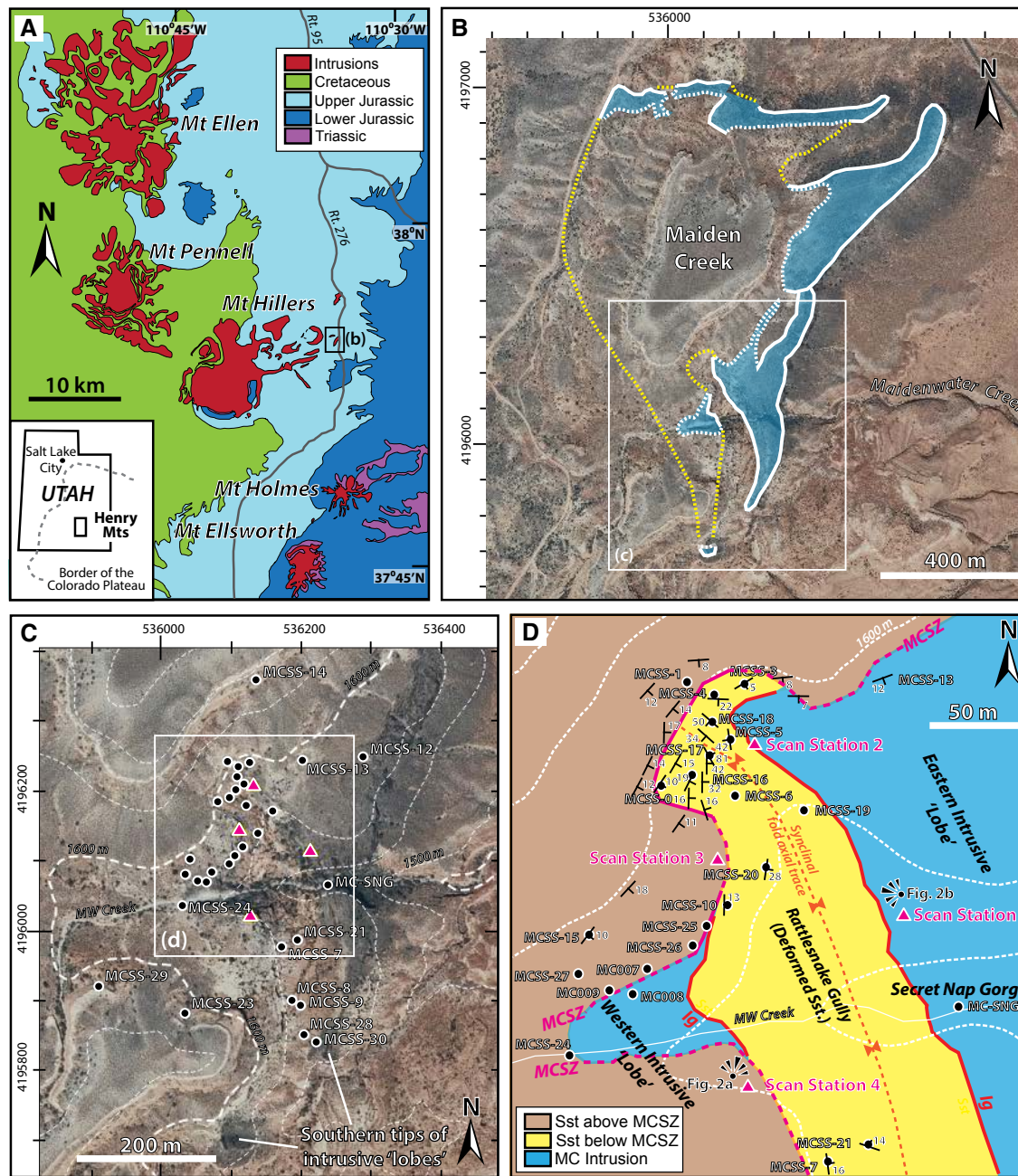


Figure 1. Maps of Henry Mountains, Maiden Creek Intrusion, and study area. (A) Simplified geologic map of the Henry Mountains region and its location within Utah (from Wilson et al., 2016; adapted from Morgan et al., 2008). (B) Aerial photograph over the Maiden Creek intrusion, a satellite intrusion to the Mount Hillers Complex (see 1A). The extent of the igneous outcrop is shown in blue, while proposed subsurface outline intrusion (Horsman et al., 2005) is depicted by the yellow dashed lines. Solid white lines show steep intrusion-sandstone contacts (lateral edges), while dashed white lines show subhorizontal contacts (intrusion top surface overlain by sandstone). (C) Aerial photograph of the study area around the two southern intrusive "lobes" (area highlighted in 1B). Topographic contours every 25 m, bold every 100 m. (D) Geologic map of the northern section of the gully (area highlighted in 1C). Shear zone depicted by pink line; lateral intrusion contacts in red. Structural stations (field localities) are shown by black circles with white outlines (see also Google Earth™ kmz file in Supplemental Materials 1 [text footnote 1]); laser scan stations are shown by pink triangles; bedding measurements shown in black. Note viewpoint locations for panoramic photographs in Figure 2. MCSZ—Maiden Creek shear zone; Sst—sandstone.

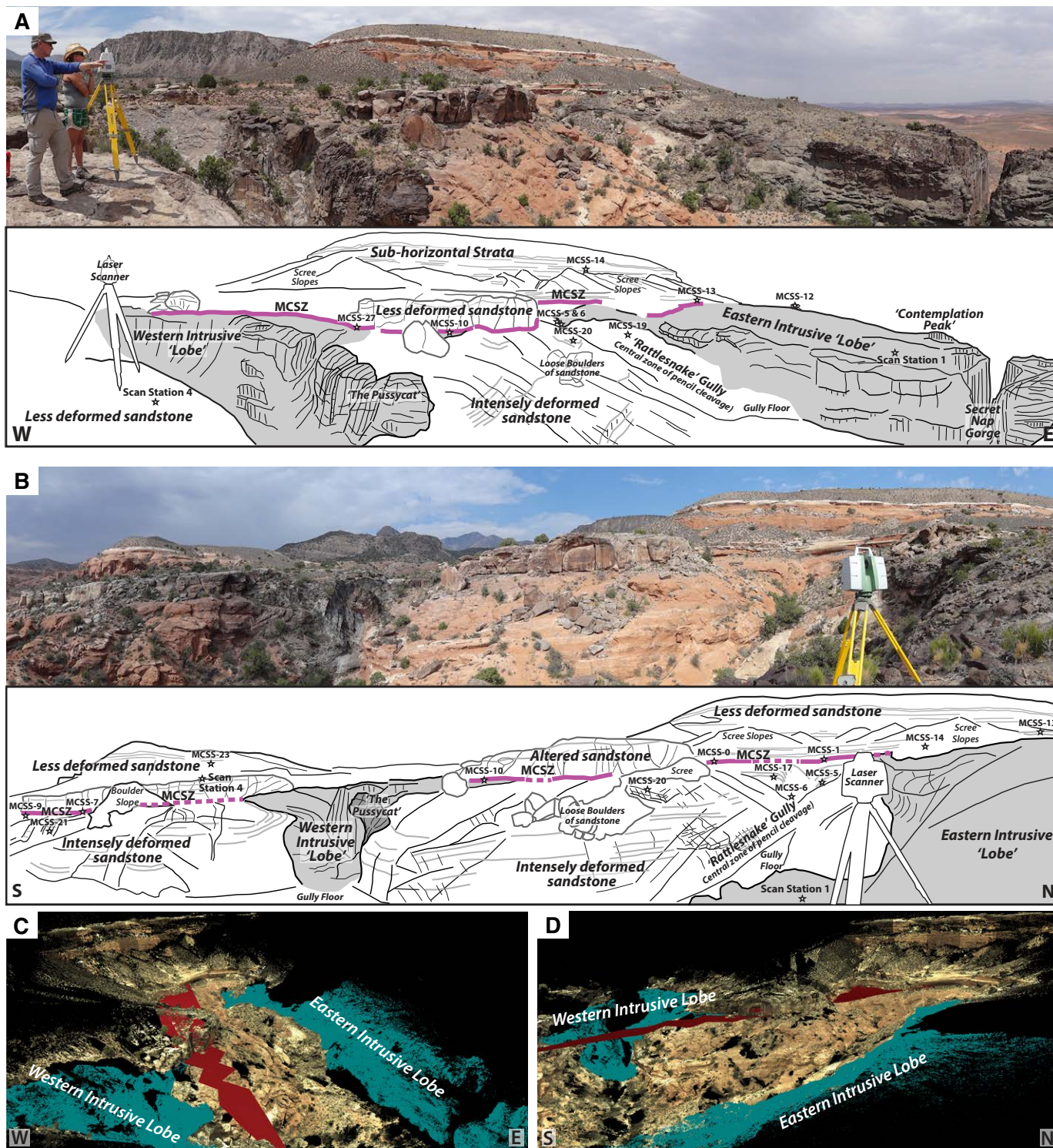


Figure 2. Panoramic photographs, annotated sketches, and laser scan models showing outcrop geometries of the study area. (A) View from scan station 4, looking north. (B) View from scan station 1, looking west. (C and D) Screen captures from 3D laser scan models (in RiSCAN PRO) showing extent of igneous outcrop (teal color) and extrapolated surface of Maiden Creek shear zone (MCSZ). Orientations roughly correspond to panoramic photograph views in (A) and (B). See Figure 1D for photograph and scan station locations.

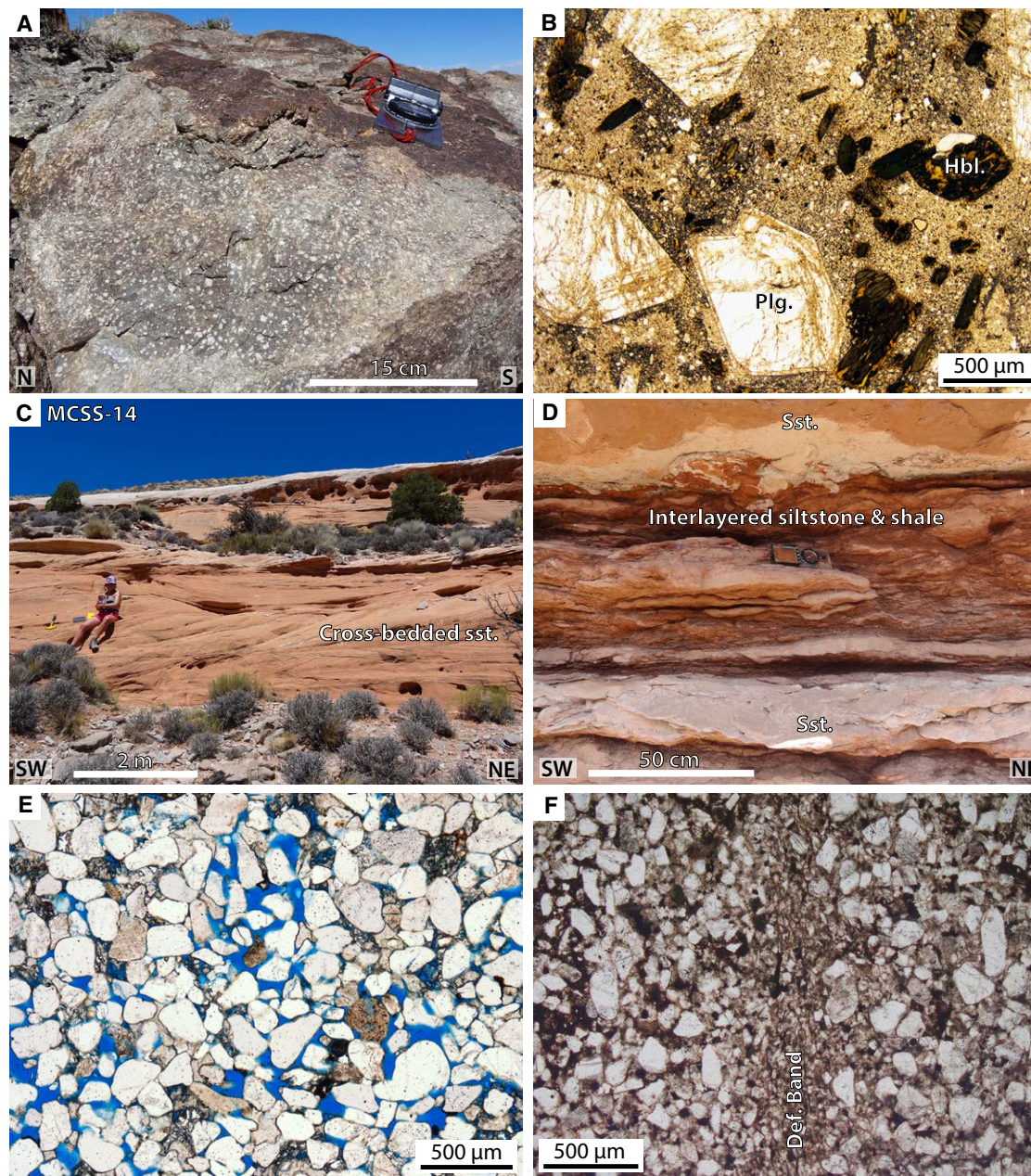


Figure 3. Field and thin-section photographs of study area lithologies. (A and B) are of the Maiden Creek intrusion. (C–F) are of the Entrada Sandstone Formation (host rock). (A) Outcrop example of freshly exposed intrusion surface showing undeformed porphyritic texture ~10 cm below intrusion top surface. (Note: Compass-clinometer is resting on chilled intrusion top surface.) Sample shown in (B) is from an equivalent outcrop to this. (B) Photomicrograph (at 5x magnification, plane polarized light [PPL]) of an undeformed intrusion (intermediate plagioclase-hornblende porphyry) sample collected from the Maiden Creek study area. Note large (0.5–5 mm) euhedral zoned plagioclase (Plg.) and smaller (0.1–0.5 mm) hornblende (Hbl.) phenocrysts in a fine crystalline matrix. (C) Outcrop photograph showing white and red cross-bedded aeolian Entrada Sandstone around Maiden Creek. (D) Example of thin interlayered siltstone and shale beds between two sandstone (Sst.) horizons (protolith to the Maiden Creek shear zone). (E and F) Photomicrographs of: (E) undeformed Entrada Sandstone showing significant porosity (blue dye) taken under PPL; and (F) example of deformed Entrada Sandstone sampled ~1 m above the top surface of the Maiden Creek intrusion (note grain-size reduction due to cataclastic deformation and calcite cementation infilling pore space).

However, narrow (<1 cm) discrete shear zones have also been identified within the intrusion (Horsman et al., 2005). In these shear zones, stretching of feldspars is apparent, reflecting local deformation in the solid state.

2.3. Host Rock—Entrada Sandstone Formation

The Entrada Sandstone is composed of white and red cross-bedded aeolian sandstones and red and brown silty sandstone beds (Fig. 3C), interlayered with thin siltstone and shale beds (Fig. 3D; Aydin, 1978). Petrographic analysis of the Entrada Sandstone in the Maiden Creek area suggests that the sandstone is subarkosic (Fig. 3E) with dominant quartz grains (>90%) and minor feldspar (plagioclase and microcline) and lithic fragments (~5%–10%). The average grain size is ~0.15 mm (Fig. 3E), although larger grain sizes are measured in some layers (Aydin, 1978). Undeformed Entrada Sandstone is highly porous, with porosities ranging between 15%–35% (Fig. 3E). Cementation is patchy (~3%–5% of the rock), with calcite spar being the most common cement (Fig. 3E), although Aydin (1978) also reported siliceous and pelitic cements within some layers. The highly porous sandstone is ideal for the formation of compactional and cataclastic deformation bands (Fig. 3F; Aydin, 1978; Aydin and Johnson, 1978; Aydin and Johnson, 1983; Fossen et al., 2007), which can help to record even quite modest strains related to magma emplacement processes (Morgan et al., 2008).

3. GEOMETRY OF THE MAIDEN CREEK INTRUSION

3.1 Fieldwork Methodology

Detailed kinematic and geometrical analyses were carried out at numerous outcrops across the study area (Figs. 1C and 1D). At each structural station, a representative structural data set was collected, including: deformation type; geometry; kinematics; phase and timing; and character. A minimum of 30 measurements were recorded per structural station (>50 in areas of high intensity deformation). In addition, oriented samples of key structures and rock units were collected for thin sectioning and petrographic and microstructural analyses.

The geomorphology and intrusion–host-rock geometries in the bedrock of the southern Maiden Creek study area are highly complex and difficult to visualize from description alone. It is also difficult to capture the 3D geometry, structural complexity, and spatial distribution of the geological observations using conventional mapping methods. Digital mapping and virtual outcrop methods have the capability to help with visualizing complex structures and to aid in the integration of multiple, spatially accurate data types (e.g., Bellian et al., 2005; McCaffrey et al., 2005; Buckley et al., 2008; Jones et al., 2009a, 2009b; Wilson and McCaffrey, 2013). Terrestrial laser scanning (TLS) acquisition, processing, and interpretation, although time consuming and expensive, have helped in the creation of a 3D structural framework as well as providing

a useful virtual image of the outcrop (Fig. 2 and fly-through movie in Supplemental Materials 2³).

TLS was carried out at four scan stations (Fig. 1C), using a Leica ScanStation C10, to acquire color point-cloud data that were georeferenced using AshTech Pro 3 DGPS data sets (Fig. 2). A combination of rapid, low-resolution (360° view angles) and high-resolution laser scans of intrusion contact zones in the southern Maiden Creek study area were acquired over the period of one day. Structural interpretation of the laser scan data helps create a 3D geological framework model of emplacement-related deformation structures and their relationship to the overall geometry of the exposed intrusion (Fig. 2). TLS also aided the capture of fracture and bedding geometries from inaccessible outcrops. The laser scan data were sufficiently detailed to also allow the spatial variation of fracture attributes to be measured (e.g., fracture geometry, connectivity, and spatial correlation).

3.2. Mesoscale Intrusion–Host-Rock Geometries

The topography of the area is dominated by two gullies. The first is a roughly N–S–trending gully (Rattlesnake Gully; Figs. 1D and 2) that is geologically controlled, flanked on either side by exposures of igneous rock with steeply dipping and highly eroded sandstones sandwiched in-between (Fig. 2). The second is a narrow E–W–trending gully—a more recent geomorphological feature formed by incision of the Maidenwater Creek (Fig. 1).

Cropping out to the east of Rattlesnake Gully is a continuous, elongate, roughly N–S–trending, ~400-m-long ridge composed of igneous rock that Horsman et al. (2005) described as a “finger-like lobe”; this ridge is referred to in this study as the *eastern lobe* (Figs. 1B–1D, 2, and 4A).

Aerial photographs show that the margins of the eastern lobe are gently curved and bow outwards and to the east (Figs. 1B–1D). The intrusion–host-rock contacts of the eastern lobe are best exposed at the head of the gully (Fig. 2). Less well exposed igneous outcrops also occur along the western flank of Rattlesnake Gully and are here termed the *western lobe* (Figs. 1B–1D and 2). The E–W–trending incision, formed by the Maidenwater Creek (Figs. 1B–1D), provides excellent 3D exposure through both the eastern and western intrusive lobes. The part of the incision cutting the eastern lobe is known locally as Secret Nap Gorge (Figs. 1D, 2A, 2B, and 4A), while that part of the incision cutting the western intrusive lobe forms an amphitheater dominated by a pillar-like outcrop known as “The Pussycat” (Figs. 2, 4B, and 4C). Within this amphitheater, the geometry of the eastern margin of the western lobe is especially well exposed: the intrusion top contact is relatively flat-lying (Figs. 4B and 4C), while the lateral contact shows a distinct angular hour-glass geometry (Fig. 4C), with upper and lower portions of the intrusion protruding further into the adjacent host rock than in the middle portion. Similar hour-glass geometry is also observed on the eastern margin of the eastern lobe. A distinct structural zonation is also apparent within the intrusive lobes: subhorizontal faults and fractures dominate the upper 5 m of the intrusion, while subvertical fractures



³Supplemental Materials 2. Fly through movie of terrestrial laser scan (TLS) model. Please visit <https://doi.org/10.1130/GES02067.S2> or access the full-text article on www.gsapubs.org to view Supplemental Materials 2.

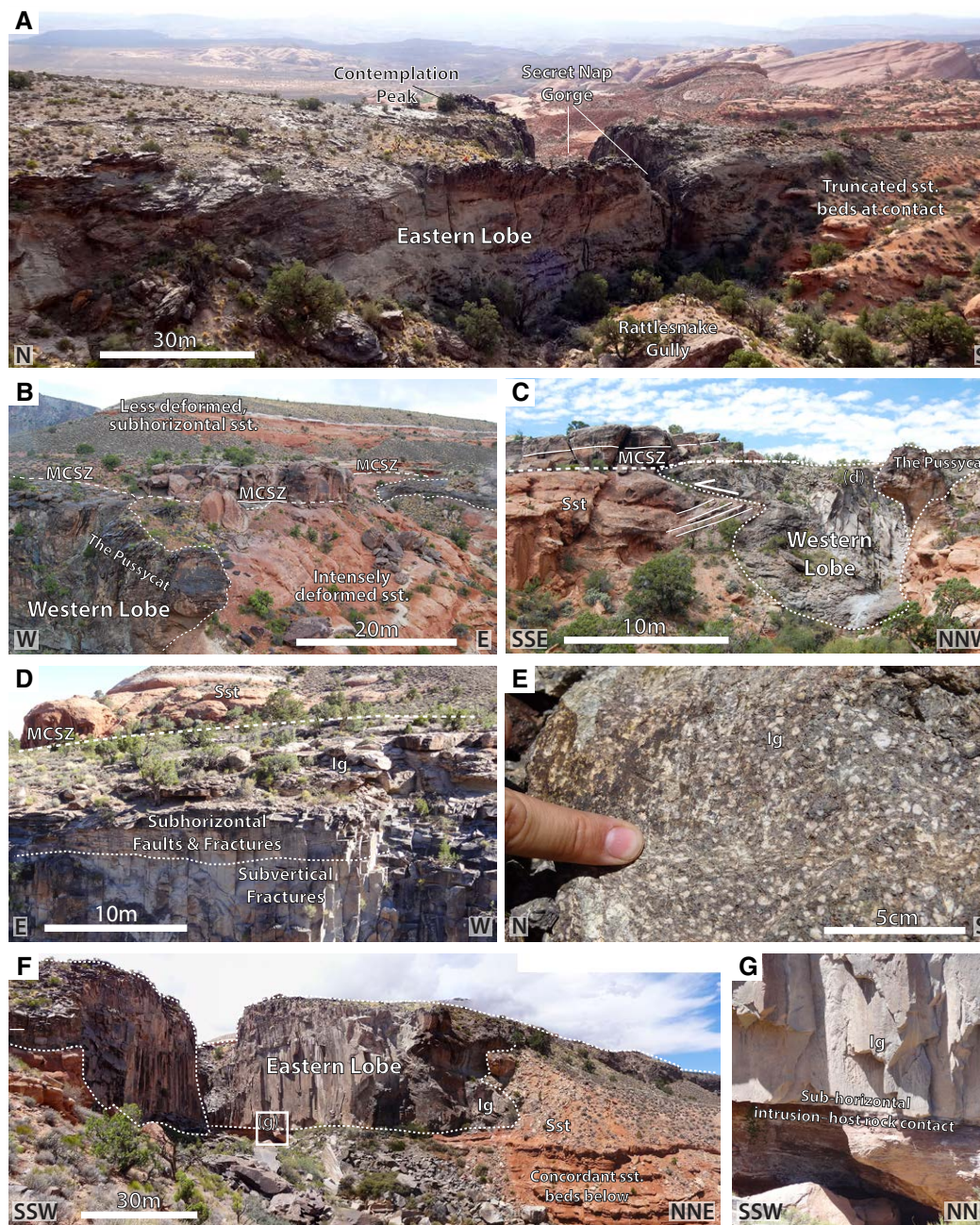


Figure 4. Intrusion outcrop geometries and fabrics. (A) The western margin of the eastern intrusive lobe (view looking east). Here outcropping intrusion is ~35 m at its thickest. Note the relatively flat intrusion top surface and narrowing toward the south. Location of Secret Nap Gorge highlighted. (B) View looking north showing the Maiden Creek shear zone (MCSZ) sitting on the top surface of the two intrusive “lobes” and the Pussycat outcrop. (C) View looking west showing irregular eastern margin of the western intrusive lobe. Note similarity in shape of the Pussycat outcrop with the intrusion geometry in the rock face to the left. (D) Structural zonation to the western lobe resulting from subhorizontal and/or low-angle faults and fractures in the uppermost few meters of the western lobe and subvertical fractures (cooling joints?) below these. Note location in (C). (E) Localized shear deformation within the intrusion, shear planes commonly subparallel to intrusion top surface. (F) View into Secret Nap Gorge and the eastern lobe, as seen from the ESE. This is the only basal (lower) contact that can be observed. Note the irregular, hour-glass geometry to lateral intrusion margin. Beds below are subhorizontal and concordant with the lower intrusion contact but are discordant (truncated) against the lateral margin. (G) Zoom-in of subhorizontal basal contact. Ig – igneous; Sst – sandstone.

predominate below (Fig. 4D). Outcrops exhibiting the basal intrusion–host-rock contact are limited. Basal intrusion–host-rock contacts are not observed in Rattlesnake Gully (Fig. 2), but a subhorizontal lower contact is seen on the outer eastern margin of the eastern lobe (Figs. 4F and 4G).

Sandstones in Rattlesnake Gully appear highly deformed (Figs. 2 and 5). This contrasts sharply with the exposures of the same sandstone units in the hillsides above (Figs. 2 and 3C) and also with those located at the same stratigraphic level outside the gully and adjacent to the outer margins of the two intrusions, which show only minor deformation. Detailed mapping shows that a subhorizontal detachment surface, the Maiden Creek shear zone (MCSZ; Fig. 5B), separates the deformed rocks in the gully from those overlying the intrusions. The bedding in the little to moderately deformed rocks above the MCSZ is shallowly dipping ($\sim 10^\circ$) to the SE (Fig. 6A). A far greater spread of measurements for bedding occurs in the gully below the MCSZ, where sandstones occur between the two intrusive lobes. Here, the sandstone bedding is folded into a synclinal structure with convex limbs—meaning that the fold tightens into the center of the gully. A subvertical fold axial plane trending \sim SSE–NNW can be traced along the center of the gully (Figs. 5C and 6D–6G).

4. DEFORMATION STRUCTURES

Deformation structures observed in the intrusion host rocks include deformation bands, faults, tensile joints, stylolites, and pencil cleavage (Figs 5–7). Deformation structures and styles change markedly above and below the MCSZ detachment surface (Figs. 5A and 5B), as illustrated by comparison of the orientation data shown in Figure 6.

4.1. Deformation Structures above the MCSZ

The gently dipping sandstone beds (Figs. 3C and 6A) above the MCSZ are commonly cut by shear and tensile fractures. Smaller offset shear fractures are *deformation bands* (Figs. 5C and 6A), characterized by narrow (mm-scale) zones of cataclasis, calcite cementation, and resulting collapse of porosity (Fig. 3F). These bands typically have a decimeter- to meter-scale spacing and represent a low- to moderate-deformation intensity (Fig. 5C). The deformation bands commonly show subcentimeter-scale normal offsets of bedding (Fig. 5C). They collectively exhibit a dominant NE–SW trend but are locally more varied in orientation and polymodal (e.g., Reches, 1987; Krantz, 1989; Fig. 6A). Larger shear fractures with clear kinematic indicators and principal slip surfaces are also observed. For the purposes of this study, we have classified these fractures as *faults*. In the sandstones above the MCSZ, these faults dominantly trend N–S and show normal dip-slip movements (i.e., E–W extension; Fig. 6A). A set of steeply dipping tensile joints trend WNW–ESE and are oriented roughly perpendicular to the deformation bands (Fig. 6A). These joints commonly have a decimeter- to meter-scale spacing.

4.2. Deformation Structures below the MCSZ

Porosity-reducing deformation bands are prolific beneath the MCSZ and are associated with the fold in the sandstones. They occur with centimeter-scale spacing immediately below the MCSZ, increasing in intensity (mm spacing) toward the synclinal hinge. In contrast to the deformation bands found above the MCSZ, strike-slip and reverse offsets of bedding are dominant here (Figs. 6E–6I). Although the orientation of deformation bands varies spatially (see below), two distinct conjugate trends are apparent: \sim SSE–NNW and \sim ENE–WSW (Fig. 6C).

Sandstone beds flanking the western intrusive lobe show stepped (kink-band) geometry as they steepen into the synclinal hinge (Figs. 5D and 5E). This occurs due to the presence of several vertical deformation band corridors trending \sim NW–SE (Fig. 5D). This stepped geometry is less apparent on the beds flanking the eastern lobe. Instead, a clear rotation of deformation bands and fractures into the fold core mimics the steepening of the beds toward the gully center (Fig. 5F).

As the intensity of deformation increases toward the center of Rattlesnake Gully, deformation bands start to take on a character more akin to a fracture cleavage (i.e., discrete fracture planes rather than narrow zones of deformation). Two distinct conjugate planes are apparent, trending SSE–NNW, parallel to the fold axis (Fig. 6C). The fold core in the center of the gully is characterized by the development of a zone of mm-scale pencil cleavage arising from the intersection of these conjugate fracture cleavage planes (Figs. 5A–5H). Pencil cleavage intersections plunge shallowly to the SSE and parallel the synclinal fold axis (Fig. 6C). Deformation intensities within the fold core are high, and bedding laminations are obliterated.

Numerous fault planes (fractures and deformation bands with clear kinematic indicators) are observed in the sandstones flanking the eastern lobe (Fig. 5I). These faults show strike-slip kinematics (from slickenlines and cm-scale offsets on deformation bands and cross-beds) and form a conjugate system of NNE–SSW dextral and ENE–WSW sinistral structures (Figs. 5I and 6C). They are consistent with NE–SW shortening and SE–NW extension. These faults are also observed cross-cutting the intrusion–host-rock contact (Fig. 7).

4.3. Deformation Structures at the Intrusion–Sandstone Contacts

Deformation structures observed at the intrusion–sandstone contacts include: strike-slip faults, mineral stretching lineations, low-angle faults, and stylolites. These structures have different spatial distributions relative to the upper and lateral margins of the intrusion.

4.3.1. Lateral Margin

The western lateral margin of the eastern lobe (i.e., within Rattlesnake Gully) is structurally controlled with sandstone flexed and truncated by a steep intrusive contact. Through detailed outcrop studies, faults can be traced continuously from

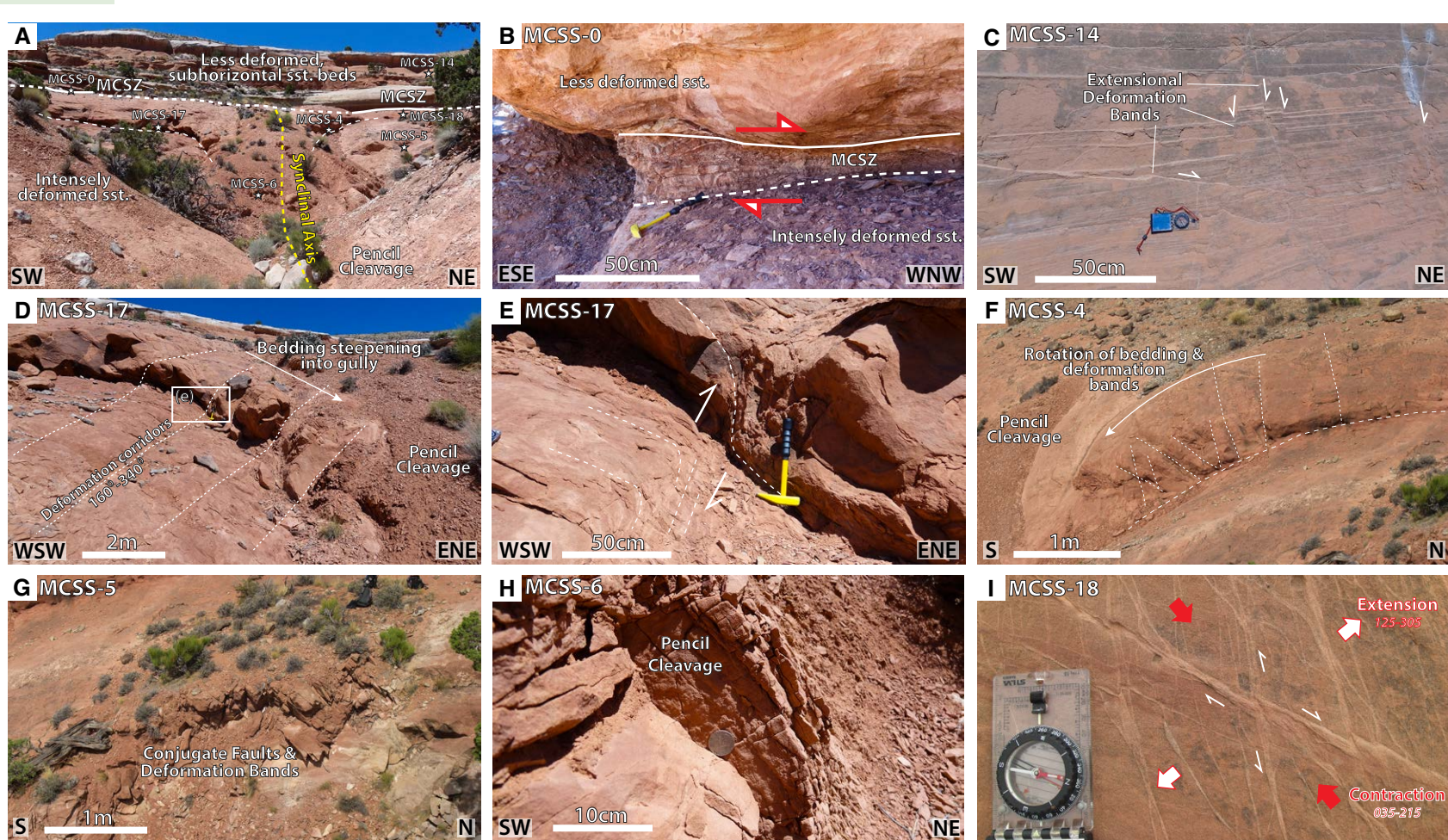


Figure 5. Field photographs showing deformation structures in the host-rock sandstones above and below the Maiden Creek shear zone (MCSZ). (A) Head of the sandstone gully (Rattlesnake Gully), view looking NW, showing low to moderately deformed subhorizontal sandstone (sst.) beds above the MCSZ, with intensely deformed and folded sandstone beds below. (B) Zoom-in photograph of the well-developed shear zone, MCSZ, outcrop (MCSZ-0). (C) Low to moderate deformation in sandstone beds ~50 m above the MCSZ with extensional offsets on bedding along deformation bands. (D) “Kink-band” geometry to deformed sandstone beds flanking the western intrusive “lobe” and increasing deformation banding with steepening of bedding into the gully; note central zone of pencil cleavage. (E) Zoom-in of (D) showing “kink-band” geometry as the folded beds pass through a vertical deformation corridor. (F) Rotation of deformation banding about a horizontal axis corresponding to monoclinical folding (note the lack of “kink-banding” observed for the western “limb”) of beds flanking the eastern intrusive “lobe.” (G) Conjugate strike-slip faults and deformation bands on beds flanking the eastern lobe. (H) Zoom-in of pencil cleavage (discrete planes) seen running along the center of Rattlesnake Gully. (I) Deformation banding displaying strike-slip offsets on other deformation bands. Note: Photograph taken in plan view.

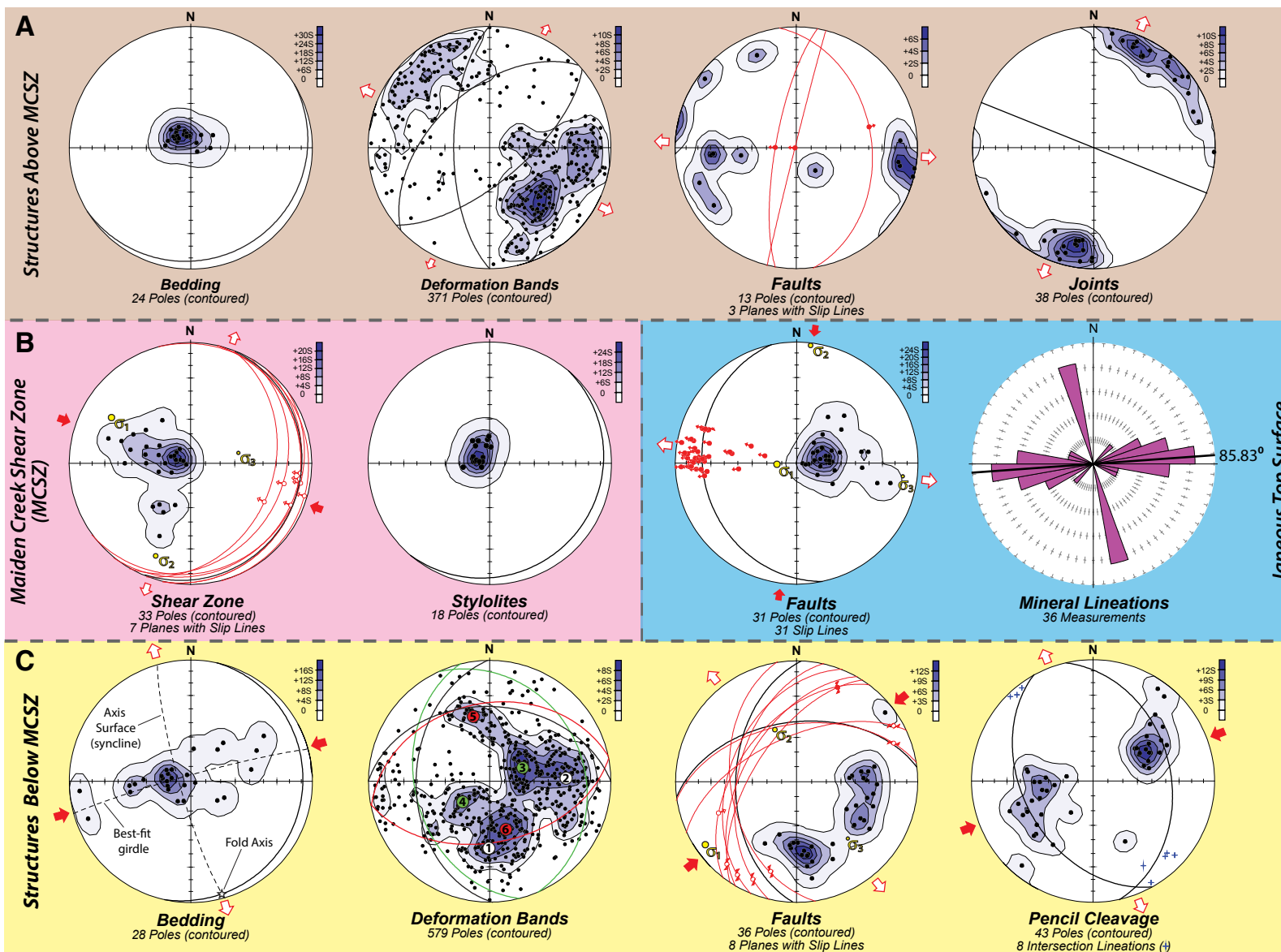


Figure 6. Summary stereoplots of field structural data. Equal area, lower-hemisphere stereoplots of data showing poles to planes (contoured) sorted by spatial location with respect to the Maiden Creek shear zone (MCSZ). (A) Bedding and deformation structures in sandstone above the MCSZ. (B) Deformation structures within the MCSZ and on the top surface of the igneous lobes (mineral stretching lineations shown in rose diagram plot; radial marks depict 5% intervals of total percentage of measurements). (C) Bedding and deformation structures in the sandstone gully below the MCSZ and between the southern igneous lobes. Mean planes for distinct cluster populations are shown for each plot. Fault and shear zone plots also show fault slip lines with movement direction indicated (red solid fill—normal fault slip; white fill—reverse slip).

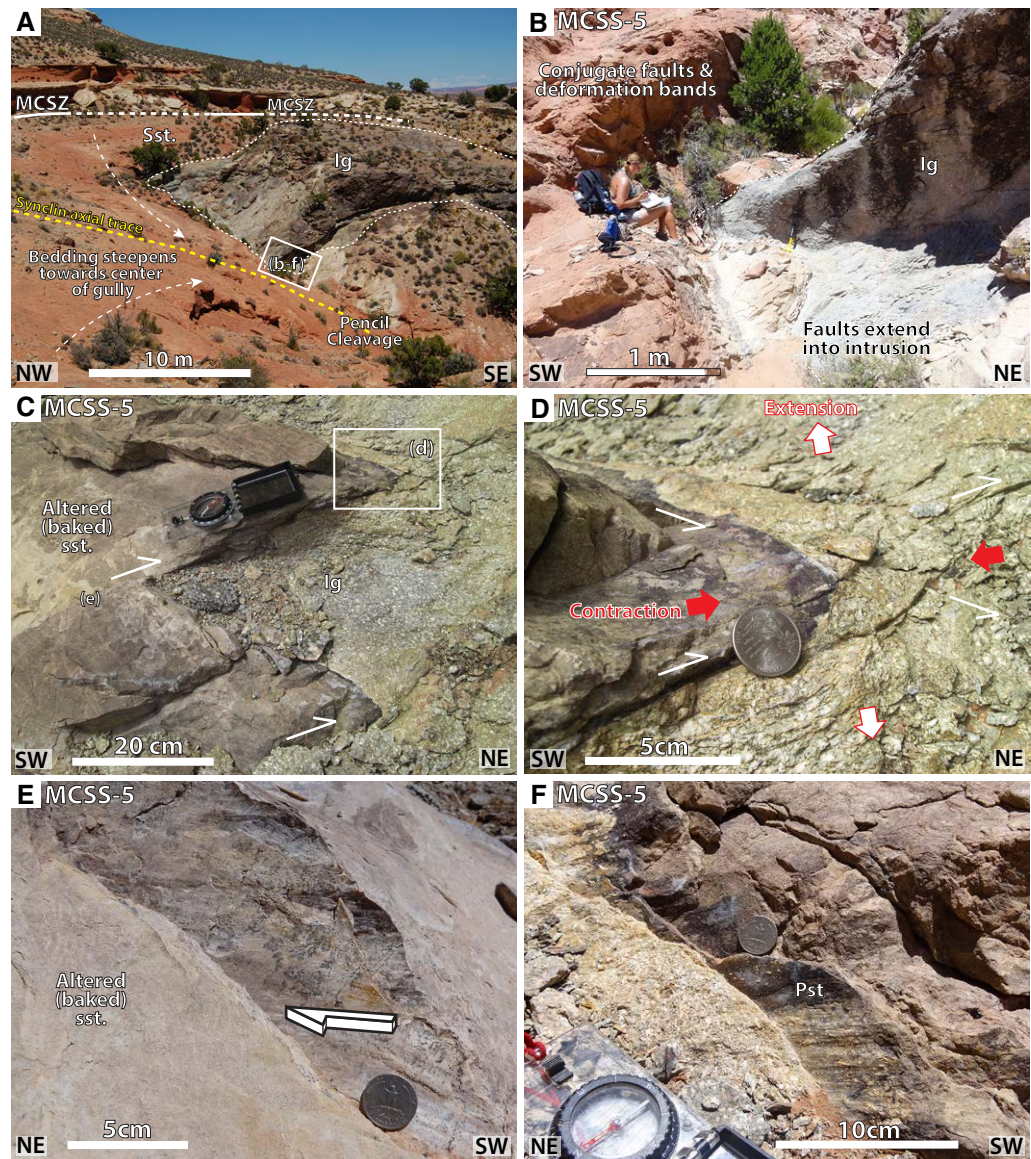


Figure 7. Field photographs showing deformation structures at the intrusion-sandstone contact. (A) Intrusion–host-rock contact along the western margin of the eastern lobe at the head of the gully. (B) Conjugate strike-slip faults in the sandstones adjacent to the eastern lobe, extending into the intrusion. (C) Stepped (jagged) intrusion–host-rock contact controlled by syn-emplacment faulting. (D) Zoom-in of (C) showing conjugate fractures in both intrusion and host rock. Note also the rounded tip to the sandstone protrusion with aligned elongate crystals in the neighboring intrusive rock mimicking the contact geometry, highlighting that structures are syn-emplacment because they were active while magma was still able to behave in a ductile phase. (E) and (F) Slickenlines indicating strike-slip movement along a fault plane within altered sandstone adjacent to the eastern lobe (E) and at the igneous-sandstone contact (F). Ig—igneous; Pst—pseudotachylyte; Sst—sandstone.

the sandstone into the neighboring intrusion (Figs. 7C and 7D). Conjugate faults trending parallel to those in the neighboring sandstone appear to control the geometry of the intrusion–host-rock contact, leading to a jagged intrusion margin (Figs. 7C and 7D). Exposed fault surfaces preserve subhorizontal, strike-slip slickenlines (Figs. 7E and 7F) at the intrusion–sandstone contact. Minerals within the intrusion are stretched and/or sheared parallel to the fault planes (Fig. 7D).

Along the eastern margin of the western lobe, similarly structurally controlled intrusion margin geometry is observed (Figs. 4C and 8). Below “the Pussycat” outcrop (Figs. 2, 4B, and 4C), faults within the sandstone can be observed dipping parallel to the intrusion contact (Fig. 8). Due to the inaccessibility of parts of this outcrop, TLS was utilized to capture fault geometries (Fig. 8C). Fault planes were constructed in GoCAD™ (Fig. 8D) from interpreted polylines (RiSCAN PRO). A set of shallowly dipping conjugate reverse faults were identified, trending SSE–NNW, consistent with fault geometries seen in neighboring accessible outcrops (Fig. 8F).

4.3.2. Upper Intrusion

Immediately below the MCSZ, a locally strong linear fabric defined by aligned, stretched plagioclase phenocrysts is developed in a narrow zone, up to 10 cm thick, located on the top surfaces of both the eastern and western intrusive lobes (Figs. 9A–9C). Two trends are observed (Fig. 5B): a dominant ~E–W trend (086°–266°), observed at multiple locations on both intrusive lobe top surfaces; and a weaker ~N–S trend. Stretched plagioclase phenocrysts are also observed along discrete subhorizontal shear bands in the uppermost 5 m of the intrusion (Figs. 4D, 4E, and 9A).

Low-angle fault planes bisect the upper few meters of the western intrusive lobe (Figs. 4D, 6B, and 9D). These fault planes trend parallel to the ~N–S strike of the intrusion margin and dip shallowly (~20°) to the west (Fig. 6B). Slickenlines and lunate fractures on these slip surfaces indicate top-to-the-west kinematics (Figs. 6B and 9D). Similar low-angle fault planes can be seen within highly altered sandstones directly above the intrusion of the western lobe (Fig. 9E). These country rock–hosted, low-angle faults exhibit a soft, white precipitate along fault surfaces, suggesting that they likely acted as fluid conduits during alteration of the sandstone.

Stylolites are observed within ~5-m-thick horizons of altered sandstone located immediately above the intrusive lobes (Figs. 6B and 9E–9G). The stylolites occur on a centimeter to meter scale and are relatively simple in character, forming a wave-like surface (Fig. 9F), dipping shallowly to the SE (Fig. 6B). They are typically oriented parallel to both the sandstone beds in which they are found and to the underlying top surface of the intrusion (Figs. 6A and 6B).

4.4. Spatial Distribution of Deformation Structures

Deformation structures and geometries vary across and along the gully (Fig. 10). The strike of the deformation structures generally parallels the trend of the nearest

parts of the eastern and western intrusive lobes; i.e., ~SSE–NNW at the head of Rattlesnake Gully, rotating to ~N–S moving to the south (Fig. 10). In the south, where the gully opens out, the sandstones only appear flanked by intrusive rocks to the west, and here deformation structures switch orientation to an ~E–W trend (see localities MCSS-28 and MCSS-30 in Fig. 10). Deformation structures throughout most of Rattlesnake Gully are contractional. However, the ~E–W–trending structures in the south display characteristics more typical of opening “mode 1” joints (i.e., extensional). These structures are oriented perpendicular to the dominantly contractional deformation bands seen within the rest of the gully (Fig. 10).

Adjacent to the eastern lobe, a number of small faults can be seen cross-cutting and shaping the sandstone–intrusion contact (Fig. 7). The kinematics on these faults appear to change, traversing from north to south along the margin. Starting in the NE of Rattlesnake Gully (Fig. 10), these faults are dominantly strike-slip faults (Figs. 5C, 6I, 7, and 10), while in the south, dip-slip reverse kinematics dominate (Fig. 10).

5. MAIDEN CREEK SHEAR ZONE (MCSZ)

The Maiden Creek shear zone is a previously undocumented thin (<1-m-thick) shallowly dipping structure that separates weakly deformed sandstone above from highly deformed sandstones (within Rattlesnake Gully) and sheared intrusive top surfaces below (Figs. 5 and 11).

5.1. Outcrop Observations and Spatial Extent

The best exposure of the MCSZ lies at the head of Rattlesnake Gully, at the base of a ~2-m-high sandstone cliff face created by the shear zone eroding more easily than the surrounding host sandstones (Figs. 5A, 5B, and 11). Here the shear zone in the sandstones is subhorizontal and characterized by a series of shallowly (<25°) ESE-dipping shear planes with ESE–WNW–trending slickenlines preserved on upper and lower shear plane surfaces (Fig. 6B). It appears to be at its thickest in this location, measuring ~0.6 m thick (Figs. 11B and 11C). On subvertical surfaces that parallel the movement direction, C-type shear fabrics (Passchier and Trouw, 2005) indicate top-to-the-WNW kinematics (Figs. 6B and 11C). The shear zone exhibits a strong foliated fabric with an interlayered sequence of thin (cm-scale) clay-rich brown layers, more competent hard red sandstone layers, and sigmoidal quartz lenses (up to 10 cm long; Fig. 11C). The lithologies here are similar to undeformed thin siltstone and shale beds observed locally within the Entrada Sandstone Formation (Fig. 3D), and it is suggested that these rocks are the most likely protolith for the shear zone materials.

The MCSZ can be traced laterally onto the top surface of both intrusive lobes, although exposures are better on the western lobe (Figs. 11D and 11E). Here the shear zone is <15 cm thick, and shear fabrics are difficult to identify due to a lack of 3D exposures and inaccessibility. However, ESE–WNW slickenlines can still be recorded on lower and upper shear surfaces (Fig. 6B).

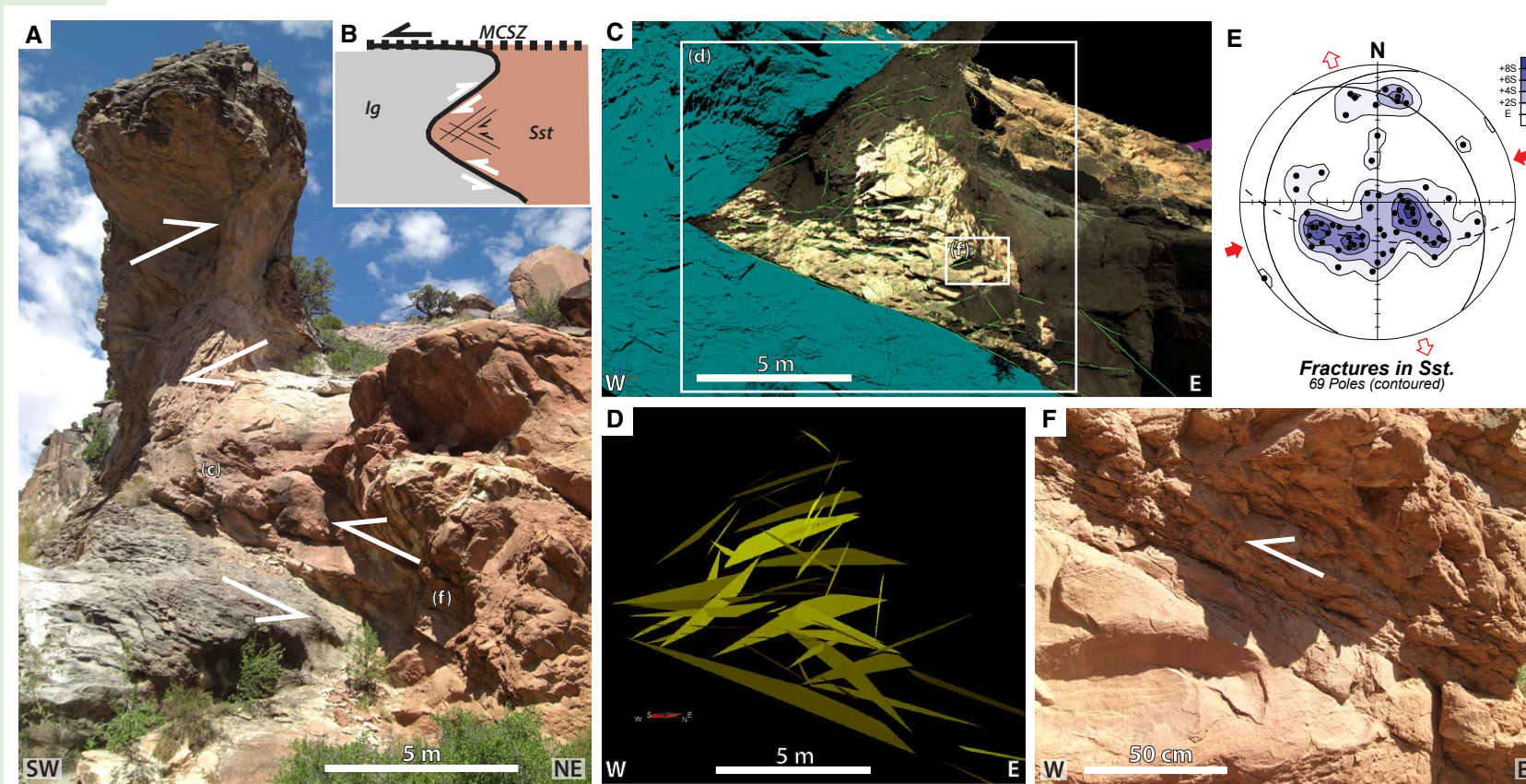


Figure 8. Pussycat outcrop geometry and deformation kinematics. (A) Outcrop photograph of the Pussycat, viewed from below (within Rattlesnake Gully). Note intrusion-sandstone contact geometry depicted by shear arrows. (B) Schematic cartoon depicting the observed intrusion–host-rock geometries observed at the Pussycat and the associated deformation structures in the neighboring sandstone units. (C) High-resolution laser scan image of the igneous sandstone contact area in the Pussycat (igneous outcrop extent highlighted by teal-colored point cloud, while color assigned to sandstone is defined from pixel color in outcrop photograph, and picked faults and fractures depicted by green lines). (D) Because access to the outcrop is difficult, fault planes were extrapolated from picked fault lines, shown in (C), to form 3D surfaces from which strike and dip values were extracted. (E) Equal-area, lower-hemisphere stereonet showing poles to planes (contoured) for fault planes derived from 3D laser scan analysis (D). (F) Outcrop photograph showing faults and fractures cutting sandstones below the Pussycat, location highlighted in (A) and (C). East-dipping faults show reverse kinematics. Sst.—sandstone; Ig—igneous.

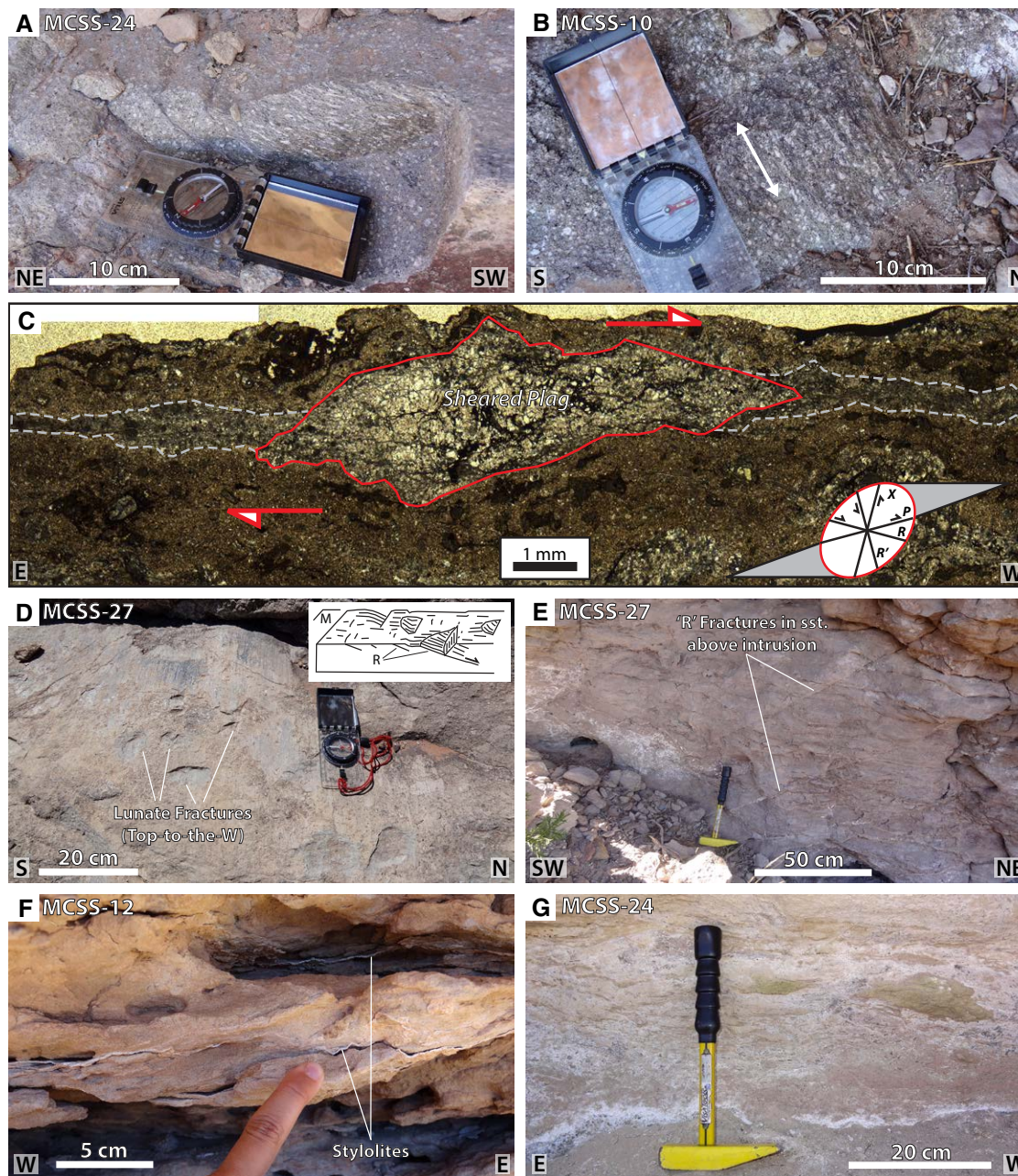


Figure 9. Field and thin-section photographs showing deformation structures on the top surface of intrusion. (A) Stretched plagioclase phenocrysts in upper 5 cm of intrusion to surface. (B) Dominant E-W fabrics of stretched plagioclase lineations on the top surface of the western intrusion, immediately below the Maiden Creek shear zone (MCSZ). (C) Photomicrograph of sheared and/or stretched plagioclase phenocryst. Note brittle deformation structures (e.g., fracturing and cataclastic flow) and top-to-the-west shear sense (kinematic indicators include: asymmetry, cataclastic deformation tails, and Riedel shear fractures). Section cut in vertical E-W orientation along axis of stretched phenocryst. (D) Low-angle faults and lunate fractures (R1 faults; inset image from Petit, 1987) indicating top-to-the-WNW movement on the intrusion top surface. (E) Low-angle faults and fractures and subhorizontal stylolites in altered sandstone (sst.) above intrusion; geometry and kinematics of faults matching those cutting intrusive rocks on the intrusion top surface. (F) Stylolites in the altered sandstone above intrusion. (G) Altered sandstones with stylolites and vein-filled fractures above western lobe (~30 m west of lateral margin), Maiden Creek shear zone (MCSZ) not clearly identifiable. Note nodular alteration zones and evidence for thermal fluid alteration.

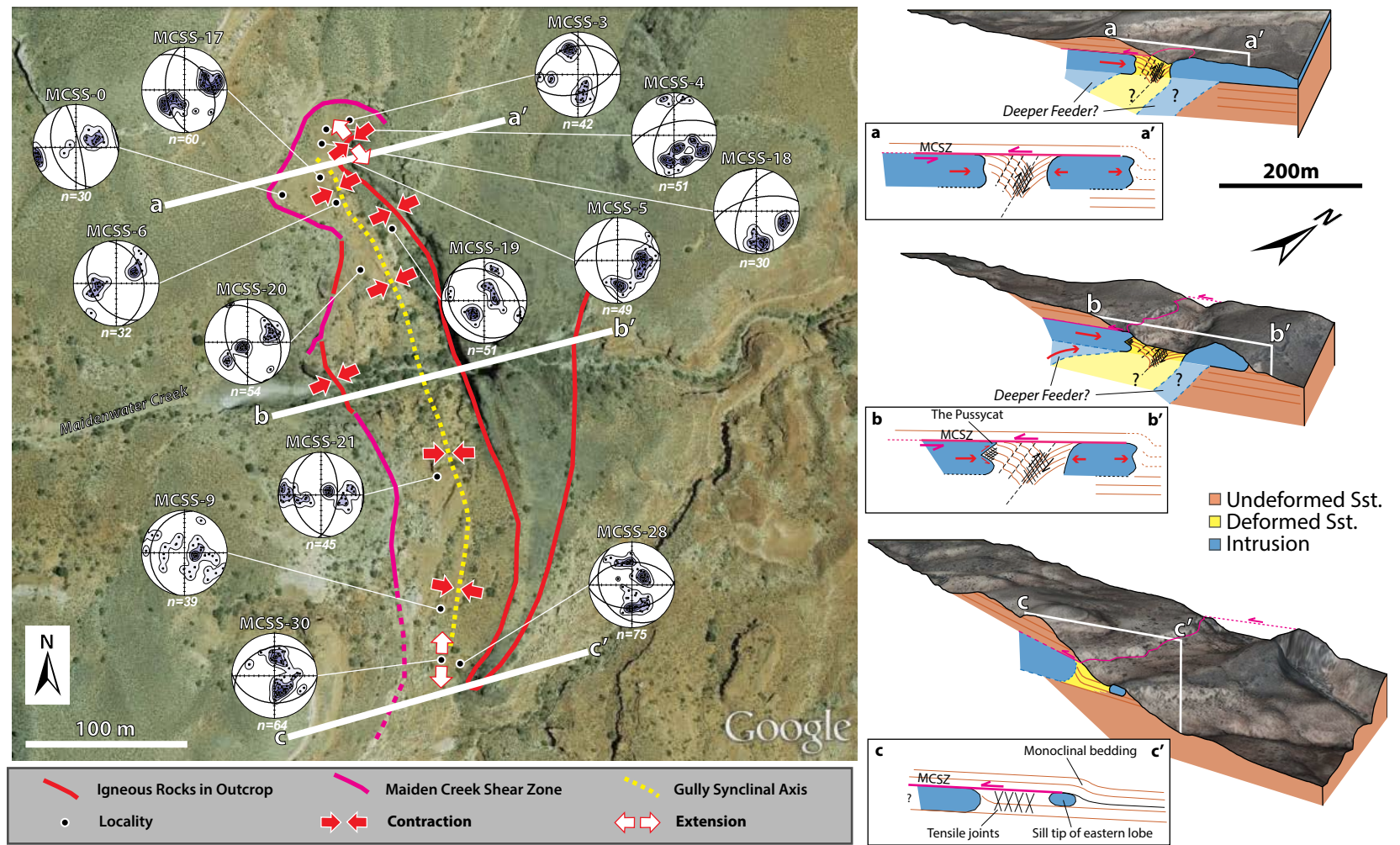


Figure 10. Spatial distribution of deformation structures across the Southern Maiden Creek study area. Aerial photograph from Google Earth™. Fault and deformation band geometries are depicted in lower-hemisphere equal-area stereoplots (contoured poles to planes and mean planes shown). Red lines depict intrusion-sandstone contacts; pink lines show mapped Maiden Creek shear zone (MCSZ); and dashed yellow line shows the synclinal axis (and associated zone of pencil cleavage). Red and white arrows depict inferred principal contractional and extensional strain orientations, interpreted from fault kinematics and structural trends. Geologic cross sections across the study area (no vertical exaggeration). Surface topography comprises an aerial photograph draped over 5 m digital elevation model surface in Move™. Inset boxes depict observed geometries, while 3D sections show potential deeper subsurface extent. Sst.—sandstone.

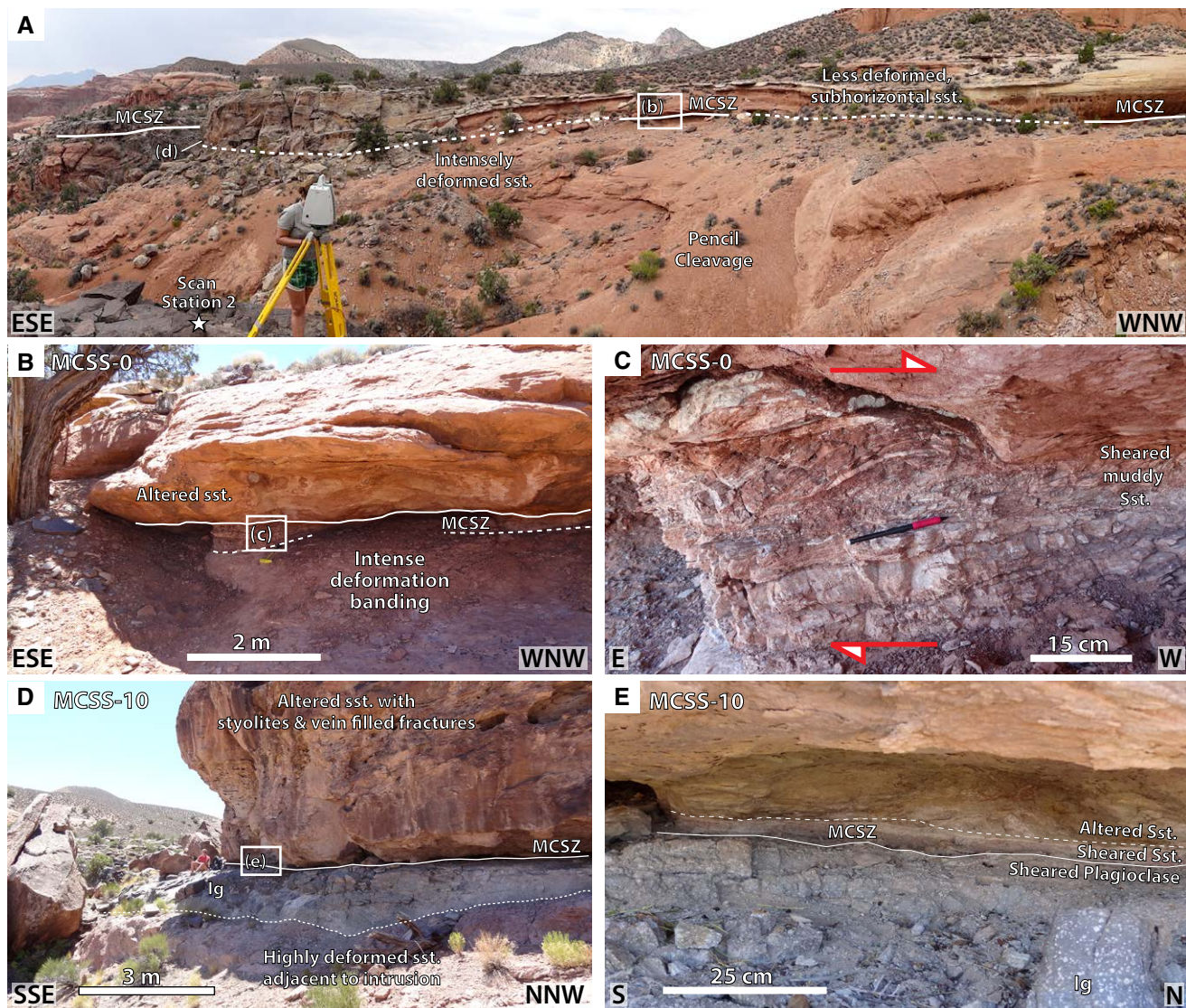


Figure 11. Outcrop photographs of the Maiden Creek shear zone (MCSZ). (A) MCSZ separating low to moderately deformed sandstone (sst.) above from highly deformed sandstone in the gully below (solid white lines depict zones where the MCSZ can be observed in outcrop, while dashed lines depict inferred continuation across areas of non-exposure). Extent of MCSZ defined in photograph is ~200 m. (B) MCSZ outcrop area in the “sandstone-sandstone domain,” locality highlighted in (A). This locality represents the best exposed area for studying the MCSZ. (C) Shear zone fabrics (C-type) observed in outcrop, showing top-to-the-west shear (area depicted in B). (D) MCSZ outcrop in the “intrusion-sandstone domain,” locality highlighted in (A). Note MCSZ is a thin deformation zone on intrusion top surface with a ~3–5-m-thick unit of altered sandstone above. (E) Thin (<5 cm) MCSZ zone separating intrusion from altered sandstone. Ig—igneous.

On the upper surface of the western lobe, a discrete shear zone becomes harder to identify. However, deformation structures consistent with the kinematics of the MCSZ are still abundant in the uppermost 5 m of the intrusion. These include the ~E–W stretched plagioclase phenocrysts and low-angle (top-to-the-west) faults in both the intrusion top surface and overlying altered sandstones (Figs. 6B and 9). These structures are all kinematically compatible with top-to-the WNW shear. Subparallel stylolites are also spatially coincident with these structures on the top surface (Fig. 9F).

5.2. Shear-Zone Microstructures

Microstructural analysis was carried out on samples collected from the MCSZ (locality MCSS-0; Figs 11 and 12). In a vertical polished section, cut normal to the shear zone fabric and parallel to the stretching lineation and movement direction (i.e., ESE–WNW), a clear layered and foliated fabric is apparent (Fig. 12A). Localized detachment surfaces (i.e., principal slip surfaces) separate broader, more distributed zones of deformation. These zones of deformation appear to reflect a distinct lithological layering, with quartz-dominated (sandstone) layers dispersed between layers of clay- and feldspar-rich (shale and siltstone) zones (white and brown layers, respectively, in Fig. 12).

Deformation microstructures within these different zones include: inclined fault surfaces and tensile fractures (Fig. 12B); S–C fabrics (Figs. 12C–12E); pressure solution seams and development of fibrous overgrowths (Fig. 12E); winged objects (σ -type porphyroclasts; Figs. 12C, 12E, and 12F); and zones of ultra-cataclasis. A number of different shear fabrics and kinematic indicators are apparent. Both C-type (Figs. 12C and 12E) and C'-type (Fig. 12D) shear fabrics can be identified. Tails of cataclastic material are also observed adjacent to some larger clasts (Figs. 12E and 12F). These all show non-coaxial deformation with a top-to-the-WNW shear sense, consistent with field observations.

Grain-scale deformation mechanisms appear to be dominated by brittle fracture, cataclastic flow, and fluid-assisted pressure solution, the latter leading to the development of the distinct foliation. Cataclastic deformation appears to predominate in the quartz-rich (sandstone) layers, although brittle faults and tensile microfractures are apparent throughout.

Microstructural analyses of sheared and stretched plagioclase feldspars within the top surface of the intrusion also demonstrate asymmetry with tails and Riedel shear fracture planes consistent with a top-to-the-WNW shear component (Fig. 9C). Deformation mechanisms again are dominantly brittle (e.g., fracturing and cataclastic flow).

5.3. Variations in Deformation Character

As outlined above, the style of deformation associated with the MCSZ appears to vary spatially across the top surfaces of the lobes (Fig. 13). Two distinct domains are recognized: (1) the *sandstone on sandstone* domain (as seen

in Rattlesnake Gully); and (2) the *sandstone on intrusion* domain on the top surface of the igneous “lobes” (Fig. 12).

In the “sandstone on sandstone” domain, the MCSZ is characterized by sharp, well-defined principal slip surfaces located at the top and base of a discrete horizon of shear fabrics, typically >0.1 m and <1 m thick (Figs. 11 and 13). In the “sandstone on intrusion” domain, deformation associated with the MCSZ is partitioned across the intrusion–host-rock contact (Fig. 13) into zones dominated by pure shear/flattening (i.e., stylolites; Fig. 9F) in the altered host rock, interlayered with zones of simple shear (i.e., sheared plagioclase; Figs. 9A–9C) found within the uppermost few meters of the intrusion. As a result, deformation here is more dispersed and is characterized by a thicker deformation zone up to ~3 m thick on either side of the top surface of the intrusion, with a less clearly defined principal shear zone (Fig. 13).

6. DISCUSSION

6.1. MCSZ: A Syn-Emplacement Accommodation Structure

The MCSZ appears to be a significant structure localized along the upper contact of the southern Maiden Creek intrusion and is associated with both the eastern and western intrusive lobes. It appears to also define an upper limit to intrusion-related deformation of host-rock sandstones within Rattlesnake Gully (Figs. 5 and 13).

Low-angle faults on the intrusion top surface show consistent top-to-the-WNW shear, matching that of the MCSZ (Figs. 6B and 9D). These low-angle faults can only be seen cutting the uppermost few meters of the intrusion. Below this, subvertical fractures predominate (Fig. 4D). As these brittle faults cross-cut the intrusion, a post-emplacement timing could be inferred. However, similar faults can also be identified in the altered sandstone immediately above the intrusion. Carbonate precipitation along these faults in the altered sandstone indicates that they were present while the intrusion was still hot enough to be driving hydrothermal fluids through the host rock. Assuming, therefore, that these low-angle faults in both the intrusion and the sandstones are contemporaneous in age, a syn-emplacement timing is likely for these structures.

The field relationships suggest that the MCSZ in Rattlesnake Gully and its continuation along the top surfaces of the intrusive lobes is consistent with it being a syn-emplacement structure. Further evidence in support for this timing comes from the lack of offset between the thermally and chemically altered overlying sandstones (Figs. 9E–9G) with respect to the underlying intrusive bodies. If the MCSZ postdated emplacement of the intrusive bodies, we would expect to see a top-to-the-west offset of the altered sandstones relative to the underlying intrusive lobes. This is not observed, and the spatial distribution of altered sandstone units corresponds very closely to the location of the top of the intrusion (Fig. 13).

Horsman et al. (2005) identified a strong relationship between mineral stretching lineations and anisotropy of magnetic susceptibility (AMS) fabrics

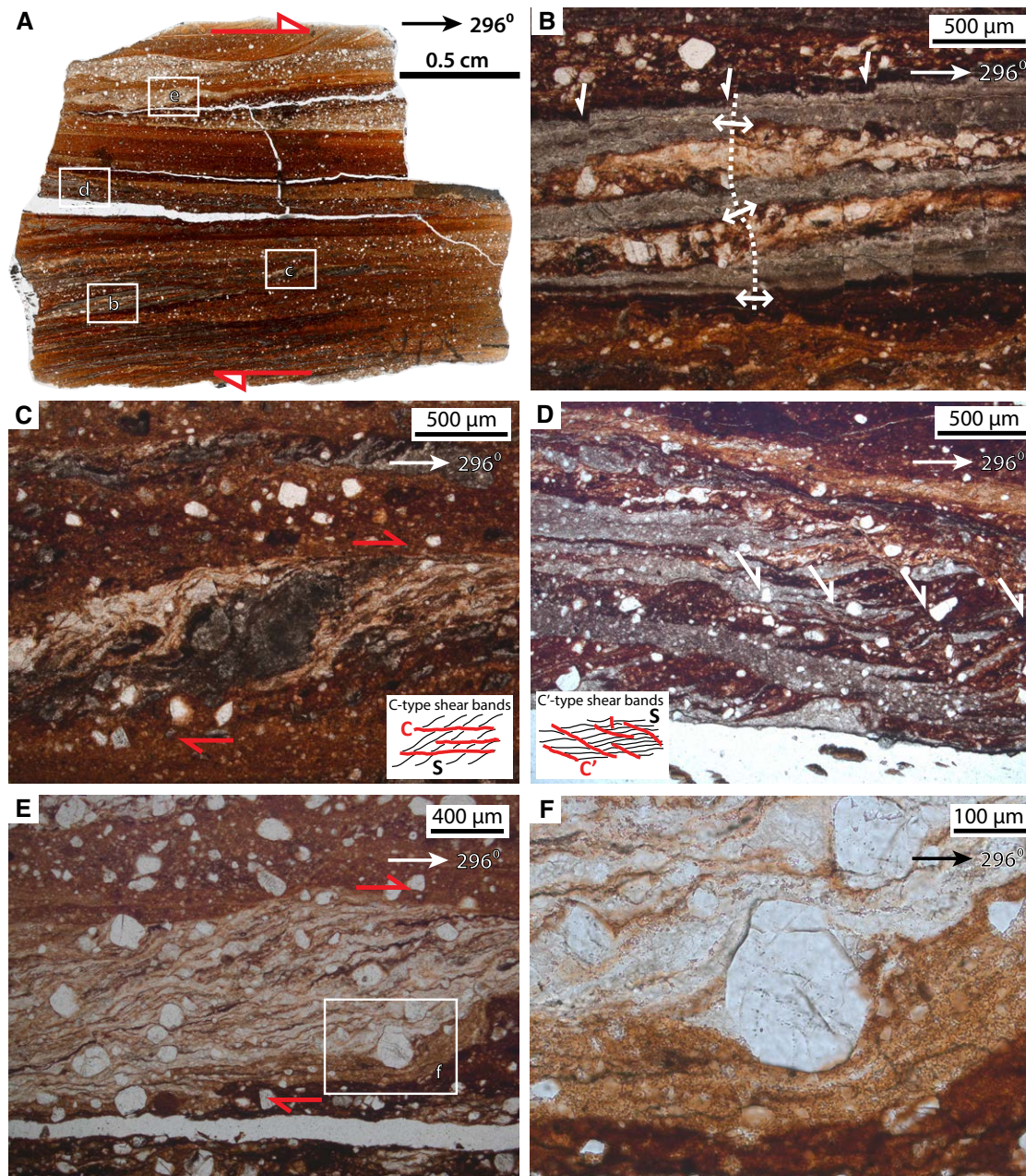


Figure 12. A series of photomicrographs of Maiden Creek shear zone (MCSZ) microstructures and fabrics, all indicating top-to-the-WNW movement. (A) Thin-section photograph of sample collected at locality MCSS 0. Note localized detachment surfaces and broader zones of foliation. Labeled boxes indicate locations of photomicrographs in (B–F). Section cut in a vertical plane parallel to transport direction (ESE–WNW). (B) Varying shear layers offset by antithetic brittle microfractures and faults. (C) C-type shear-band fabrics. (D) C'-type shear-band fabrics. (E) Cataclastic tails to quartz grains forming sigmoidal lenses. (F) Zoom-in of deformed quartz grain in (E).

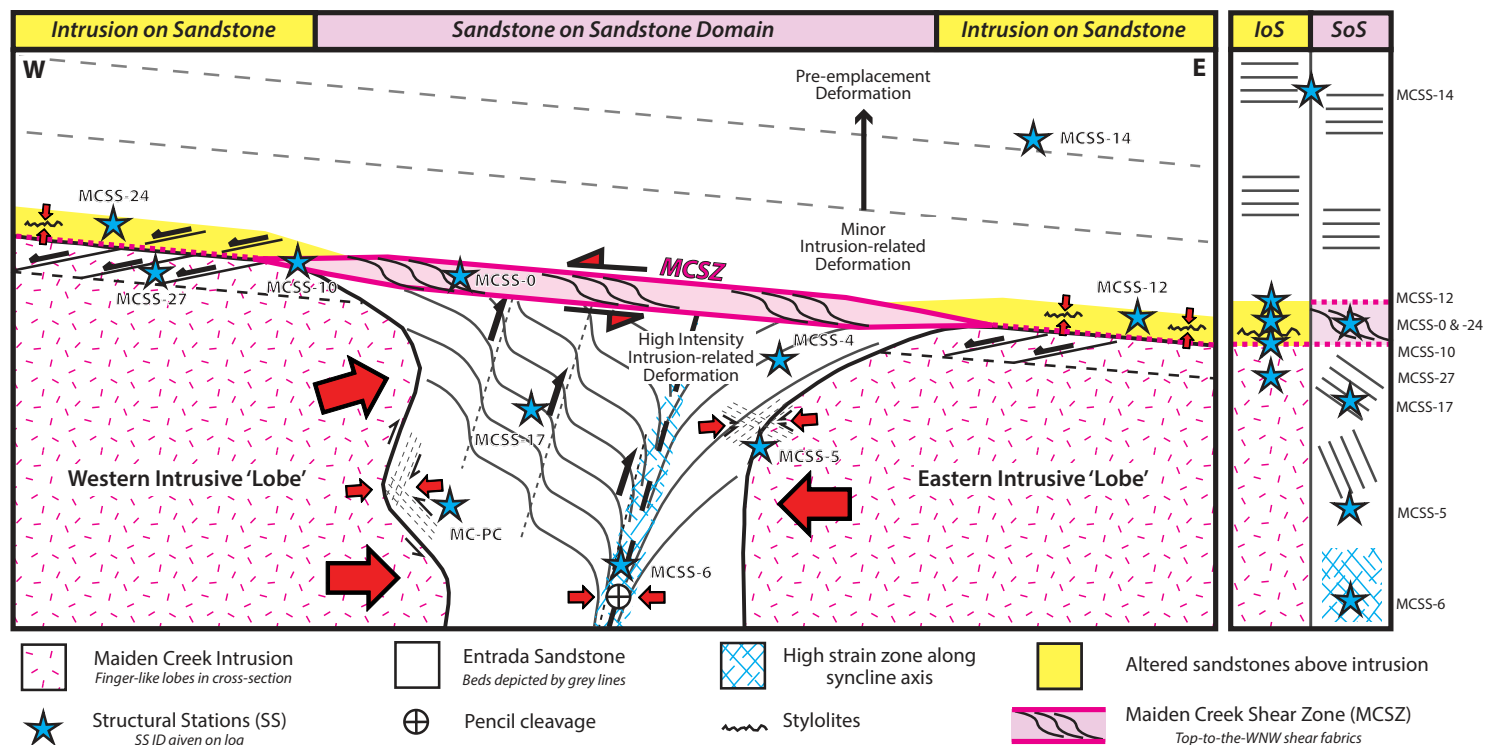


Figure 13. Schematic cross section showing spatial distribution of deformation structures in the study area. Note zonation of the Maiden Creek shear zone (MCSZ): yellow zones depict intrusion on sandstone domain (loS), while pink zone shows sandstone on sandstone domain (SoS).

in the Maiden Creek intrusion. They used these fabrics to infer magma flow directions. Horsman et al. (2005) identified both ~N-S- and ~E-W-trending fabrics on the eastern and western intrusive lobes (Fig. 14) but favored a north-to-south magma flow direction in their emplacement model. In contrast, although some N-S-trending mineral lineations are identified in our study, the field mineral lineation and kinematic data collected are predominantly E-W. The dominant E-W-trending fabrics within the intrusive lobes, along with the top-to-the-WNW kinematics observed in the MCSZ, could be explained by easterly directed magma flow, which is in turn compatible with the regional model of a feeder system to the west for the wider Maiden Creek intrusion (Horsman et al., 2005, 2009; Wilson, 2015). An easterly magma flow direction would also be consistent with the arcuate trend observed for the intrusive lobes and intervening zone of country rocks in Rattlesnake Gully.

An alternative model for the development of the MCSZ is that it is simply a décollement or gravity-driven basal detachment surface, where the less

deformed rocks above are sliding down dip due to the growth of the underlying intrusion. However, the movement on the shallowly ESE-dipping shear zone is up dip (top-to-the-WNW), and therefore, this model appears unlikely in the absence of any evidence for a later regional tilting. Furthermore, as the spatial distribution of the shear zone appears localized to the southern Maiden Creek intrusion, a regional décollement and/or detachment surface model is less likely.

6.2. Structural Complexity and Variations in Strain within Rattlesnake Gully

The spatial distribution of deformation structures and geometries in the sandstone below the MCSZ and between the two intrusive “lobes” likely reflects variations in strain within sandstones that are now exposed in the gully.

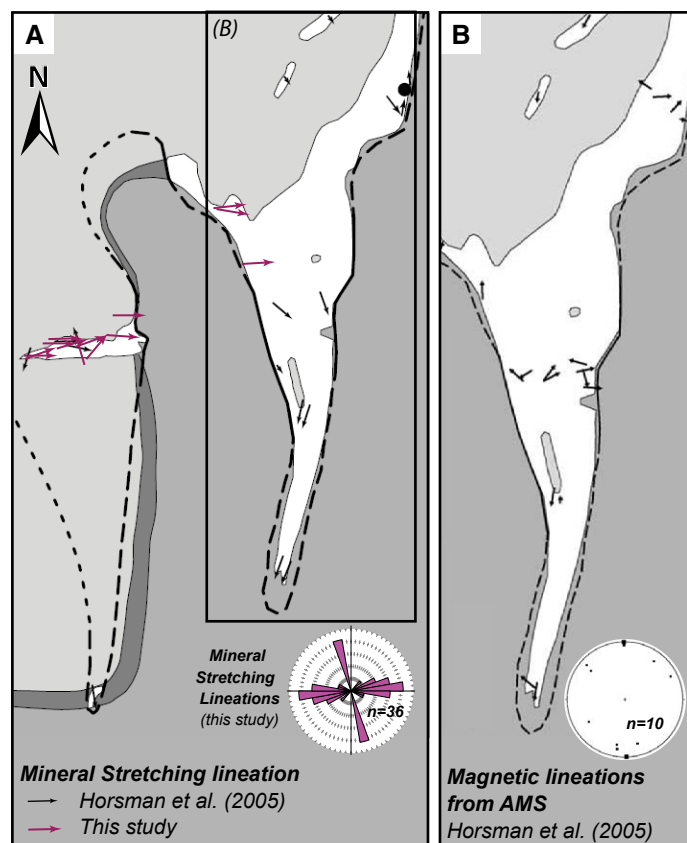


Figure 14. Spatial distribution of intrusion fabrics across the study area. (A) Mineral stretching lineations from Horsman et al. (2005) with data from this study shown also in purple and on the inset rose diagram. (B) Magnetic lineations from anisotropy of magnetic susceptibility (AMS) data for the Eastern Intrusive Lobe (from Horsman et al., 2005).

The strikes of structures in the sandstones within Rattlesnake Gully parallel the intrusion margin of the eastern lobe. Deformation is dominantly constrictional, with shortening perpendicular to the synclinal fold hinge line and intrusion margins (Fig. 10), resulting from “squeezing” of the sandstone between the western and eastern lobes. Thus, the maximum principal strain orientation rotates from ~ENE–WSW at the head of the gully in the north, to ESE–WNW in the south (Fig. 10). However, in the NE part of Rattlesnake Gully, strain is more complex, with a conjugate set of strike-slip faults observed in sandstones adjacent to the lateral margin of the eastern lobe (Figs. 5l and 10). The shortening axis associated with these conjugate sets is however still consistent with the strain axis observed along the rest of the gully.

East–west–trending extensional structures observed in the southern part of Rattlesnake Gully are perpendicular to the dominantly constrictional deformation bands seen to the north (Fig. 10). This localized zone of extension-dominated deformation is coincident with the southern tip of the eastern lobe. Therefore, changes in strain and deformation trends may reflect changes in the boundary conditions around the intrusion contacts: i.e., more contraction in the north where sandstones are trapped between two thick (>30 m) intrusive lobes and more extension in the south where the sandstones are less constrained due to the thinning (<10 m) and termination of the eastern lobe (Fig. 10).

6.3. Implications of MCSZ for Emplacement Models and Geometry of the Southern Maiden Creek Intrusion

Figure 15 provides a range of models for the emplacement and geometry of the southern Maiden Creek intrusion. Models 1 and 2 are end-member models, while a hybrid of these is also considered. Model 1 follows that proposed by Horsman et al. (2005, 2009) for the emplacement of two N–S–trending finger-like lobes. In this model, magma propagates in a southerly direction from a main “sill-like” intrusive body situated to the NW. In contrast, Model 2 involves both the eastern and western intrusive bodies propagating from depth in the WNW toward the ESE as inclined sheets, with magma flow laterally splaying from the dominant SW–NE trend (and flow direction?) of the Maiden Creek intrusion. In a hybrid of these end members, the western intrusive body is derived from depth to the west (i.e., an inclined sheet, as per Model 2), while the eastern intrusive lobe propagates from the north to the south (as per Model 1).

Using interpretation of fabric data (mainly magnetic foliation and lineation results from AMS studies) coupled with field observations of linear fabrics, Horsman et al. (2005) proposed that two radial (fanning) lineation patterns are seen in the Maiden Creek intrusion. The first lies within the main body, and the second lies within the fingers. From the lineation pattern observed in the main body, Horsman et al. (2005) speculated that, although not exposed, the feeder for the intrusion should be located toward the west or southwest. The general alignment between lineation measurements and the N–S elongation of the two southern intrusive lobes (Fig. 14) was taken to indicate a southern flow of magma away from the main body out into the fingers (i.e., Model 1; Fig. 15B). Horsman et al. (2005) proposed that these finger-like lobes initially started as small protrusions along the margin of the main body, where swelling occurred as a result of local heterogeneity, such as fracture sets in the host rock. As the magma pressure rose, propagation began outwards from the main body and continued until magma at the margin of the finger ceased to have sufficient driving pressure to displace the host-rock sediments (Horsman et al., 2005). This emplacement mechanism for the finger-like lobes is similar to that proposed by Pollard et al. (1975) for fingers around the periphery of the Shonkin Sag Laccolith in Montana, USA.

In Model 1, the constrictional deformation of the country rocks exposed in Rattlesnake Gully could result from lateral expansion of one or both of the western and eastern intrusive lobes as magma propagates in a southerly direction

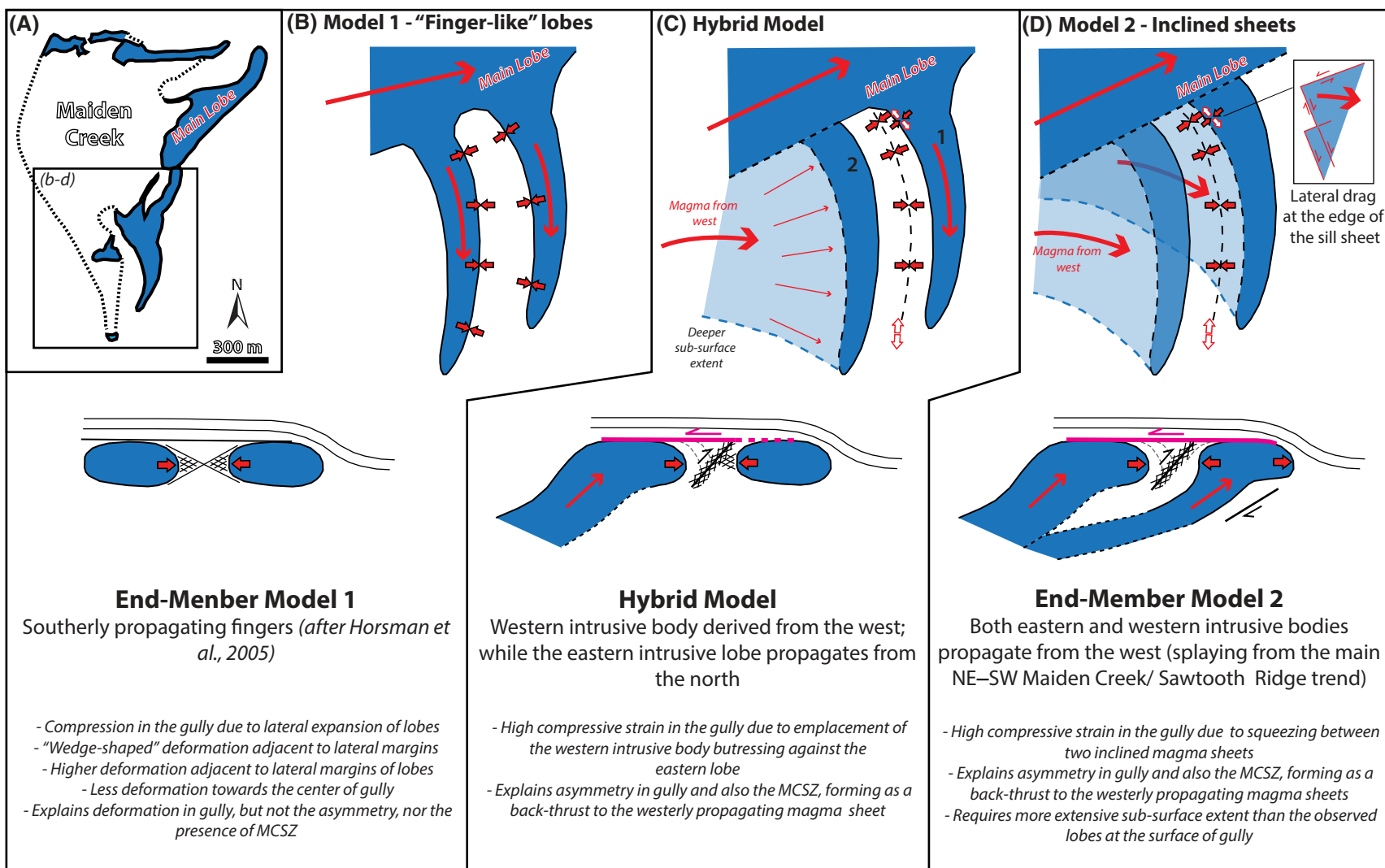


Figure 15. Three models for emplacement of the southern intrusive bodies to the Maiden Creek intrusion (see discussion in section 6.3). (A) Outline of Maiden Creek intrusion (after Horsman et al., 2005). Area covered by models proposed in (B–D) shown. (B) Model 1 assumes two southerly propagating finger-like lobes, as proposed by Horsman et al. (2005). (C) Hybrid Model has the western intrusive body propagating from the west, while the eastern intrusive lobe propagates from the north (as per Model 1). The Hybrid Model requires a more extensive subsurface to the western body than outlined in (A). (D) Model 2 involves both the western and eastern intrusive bodies propagating from a feeder system deeper to the west. This end member model requires a more extensive subsurface extent of the intrusion than suggested in (A). Models 2 and Hybrid Model both support the kinematics identified in this study. MCSZ—Maiden Creek shear zone.

(Fig. 15B). Such contraction of the host-rock sandstones trapped between would most likely lead to stronger deformation in the sandstones immediately adjacent to the lateral margins of the lobes, with deformation intensity decreasing away from the contacts. Johnson and Pollard (1973) on studying deformation structures in host-rock sandstones adjacent to and between two intrusive bodies in the NE of the Maiden Creek intrusion (i.e., the northeasterly pair of finger-like lobes in the Horsman et al. (2005) model; Fig. 15A) reported intense fracturing within a “wedge-shaped area,” as depicted in Model 1 (Fig. 15B), with fracturing extending only ~10 m into the adjacent host rocks.

Model 1, although relatively simple, does not explain the spatial distribution, asymmetry, trend, and kinematics of deformation structures observed within the host sandstones in Rattlesnake Gully. Although intense deformation banding (cm spacing) is observed in sandstones proximal to the lateral intrusion margins, in contrast to the predicted wedge-shaped zone of fracturing close to the lateral margins, deformation intensity increases toward the sandstones located in the center of the syncline (with mm spacing for discrete pencil-cleavage planes). Furthermore, in this model for lateral expansion and squeezing of sandstones trapped between two magma lobes, assuming that the emplacement of the lobes is contemporaneous, symmetrical folding and deformation would be expected (Fig. 15B), while the observed synclinal fold is markedly asymmetric as are the associated deformation structures (Figs. 10 and 13). Most significantly of all, Model 1 cannot explain the kinematics of the MCSZ, because southerly propagating magma fingers would result in top-to-the-north shear in overlying host rocks, not top-to-the-WNW as implied from field and microstructural kinematics (Figs. 6B, 11, and 12).

In order to account for both the kinematics of the MCSZ and the structural complexity observed in the sandstone beds below and in-between the intrusive bodies, we propose a new alternate model. Model 2 (Fig. 15D), with both the western and eastern intrusive bodies being fed from depth in the west and WNW (i.e., an E to ESE magma flow direction), overcomes many of the problems associated with Model 1. In this model, the western and eastern lobes are offset lobate structures that form at the leading edge of two inclined, propagating sheets that most likely coalesce at depth (e.g., a saucer-shaped sill). These lobate structures further coalesce with the main body of the Maiden Creek intrusion. In such a model, the sandstones beneath the MCSZ within Rattlesnake Gully correspond to an intervening inclined wedge (similar to a bridge structure; Magee et al., 2018). Importantly, Model 2 can account for the development and kinematics of the MCSZ, the shear zone forming antithetic to the westerly propagating magma sheets. This model works if both sheets are emplaced contemporaneously, as well as if the western body is emplaced after the emplacement of the eastern body. Lateral splaying and/or radial fanning of the magma at the tips of the upwards propagating sill sheets from the west would account for both the dominant E–W and less common N–S mineral stretching lineations (this study and Horsman et al., 2005) and AMS fabrics (Horsman et al., 2005) recorded in the eastern and western intrusive bodies (Fig. 14).

Furthermore, Model 2 explains the high constrictional strain within host rocks exposed in Rattlesnake Gully, as well as the deformation and geometric

asymmetry due to squeezing between two inclined magma sheets. The synclinal geometry and associated contractional structures within the gully imply a steeply dipping reverse-sense of shear (i.e., the western lobe propagating in the hanging wall to the eastern lobe).

A Hybrid Model (Fig. 15C) may also account for many of the geometric and kinematic observations; however, certain aspects are problematic. Not only does this model necessitate a specific order in which the eastern and western intrusive bodies are emplaced, it still requires the eastern lobe to be fed from the north (i.e., a southerly magma flow direction). Detailed structural and kinematic mapping of the greater Maiden Creek intrusion implies a dominant northeasterly magma flow direction (Wilson, 2015) for the main NE–SW–trending lobe (Fig. 1B). A north to south magma flow seems at odds with even lateral spreading from this main northeasterly magma flow direction.

Therefore, on the merits of each model in accounting for the observations in this study, Model 2, with two inclined sill sheets propagating from depth from the west, is favored. In Model 2, the observed igneous outcrop at the surface represents the steepest section at the tip of a climbing sill sheet, i.e., the frontal ramp. If the eastern intrusive body were composed of two stacked finger-like lobes, as suggested by Horsman et al. (2005), we would expect to see similar lateral bulbous geometries on both sides of the lobe. However, what we observe from the eastern intrusive body is a steeply dipping flat surface on the western lateral margin (within Rattlesnake Gully; Fig. 2), and a more irregular, eastern margin. The simpler, western margin is consistent with the upper contact of a ramp section of a saucer-shaped sill (i.e., inclined sheet). The irregular eastern lateral margins (observed for both the eastern and western intrusive bodies) are interpreted to represent the frontal tip of an upward-propagating inclined sill sheet. The irregular, hour-glass geometry of the eastern lateral margins (as seen at the Pusycat; Figs. 8 and 13) likely reflects the interaction of magma with syn-emplacment faults. Furthermore, the curved (arcuate) margin trends of the intrusive bodies may be consistent with the map-view geometry of saucer-shaped sills (Malthe-Sørensen et al., 2004; Thomson and Hutton, 2004; Polteau et al., 2008; Thomson and Schofield, 2008).

Due to lack of exposure for the western intrusive body in particular, there are uncertainties with all three models for the emplacement and geometry of the southern Maiden Creek intrusion. Further data, such as geophysical data (gravity and magnetics), are required in order to understand the subsurface extent of the intrusion and test the three alternate models for the intrusion geometry and emplacement mechanisms. However, the kinematics of the MCSZ can only be accounted for by a west to east movement of the underlying magma, contrary to the north to south magma flow inferred for the southern pair of “finger-like lobes” of Horsman et al. (2005).

6.4. The Role of Syn-Emplacement Shear Zones in Accommodating Magma

This study highlights the importance of syn-emplacment shear zones as significant accommodation structures of magma emplacement. The MCSZ, although

relatively localized, exhibits a substantial amount of strain, which likely formed in response to the forceful emplacement of the eastern and western intrusive bodies and possibly reflects the rheological properties of the highly crystalline magma during emplacement. Field data and observations support the timing of the development and movement on the MCSZ as being contemporaneous with the emplacement of the southern Maiden Creek intrusion. As such, its presence has significant implications in terms of magma flow directions, emplacement mechanisms, and subsurface intrusion geometries, the shear zone most likely resulting as an antithetic shear structure (back thrust?) to underlying magma flow.

As the MCSZ is relatively thin and spatially restricted, its presence and significance has been unnoticed in previous studies, and we suggest that similar accommodating structures may also have been overlooked for other shallow-level intrusions. Spacapan et al. (2016) identified high-strain contractional deformation structures associated with the emplacement of sill sheets in the Neuquén basin, Argentina. These deformation zones appear strongly strata bound and do not deform the overlying units, thus making these analogous to the observations in this study. We therefore postulate that an antithetic shear structure similar to the MCSZ may also exist above these high-strain deformation zones described by Spacapan et al. (2016).

Antonellini and Cambray (1992) presented a model for the emplacement of the Logan Sills (located on the northwest shore of Lake Superior, northern Ontario, Canada); in this model, magma propagated along and caused reactivation of preexisting bedding-parallel shear zones, and the overprinting shear zone indicators reflected the magma flow direction. This example represents a “pre-emplacement” accommodation structure that is locally reactivated as a “syn-emplacement” accommodation structure. The present study of the Maiden Creek intrusion highlights the importance of newly formed shear zones as “syn-emplacement” accommodation structures—localized structures formed in response to the strain induced by the intruding magma. Both examples highlight the importance of shear zones as accommodation structures.

These accommodating shear zones, whether “preexisting,” “syntectonic,” or “syn-emplacement,” are significant structures in terms of: (1) their larger size relative to other more commonly identified intrusion-related host-rock deformation structures such as deformation bands; (2) the significant amount of strain that they accommodate; (3) their role in acting as a detachment surface separating highly deformed host rock beneath and between intrusive bodies from little deformed host rocks above; and (4) the kinematics of the shear zone are strong pieces of evidence for the magma flow and propagation direction.

7. CONCLUSIONS

Host rocks to shallow igneous intrusions provide a record of emplacement and accommodation of magma in the subsurface. This study of the Maiden Creek intrusion illustrates well some of the structural complexities that may be associated with syn-emplacement accommodation of igneous intrusions with complex geometries in the shallow crust. Structural evidence in the southern

part of the Maiden Creek intrusion is consistent with westerly derived magma emplacement. Deformation structures in the host-rock sandstones that crop out within Rattlesnake Gully, between the southern intrusive bodies, are dominantly contractional (~E–W shortening), while the spatial distribution and observed asymmetry imply a reverse (east-verging) shear component. From our observations of both deformation structures and exposed intrusion geometries, we propose that the Maiden Creek intrusion in the south is composed of westerly derived inclined sill sheets, in contrast to the previously suggested model for a pair of northerly derived finger-like lobes (Horsman et al., 2005).

Overlying these deeper-rooted sills is the newly identified Maiden Creek shear zone (MCSZ). This structure, with its top-to-the-WNW shear sense, acts as a detachment surface, separating highly deformed sandstones below (i.e., between the sills) from less deformed sandstones above. Although the style of deformation in the MCSZ varies from adjacent sandstone on intrusion to the sandstone on sandstone domains, the kinematics are consistent, and there is strong evidence to support a syn-emplacement timing for the structure. The substantial amount of strain observed through microstructural analysis suggests that the MCSZ is a significant structure in accommodating magma emplacement. We believe that this is the first account of such a syn-emplacement shear zone developed on the top surface of a sill-like body that has aided the accommodation of magma.

The spatial distribution of deformation structures in the sandstones trapped between the two intrusion fingers is complex and reflects variations in strain relating to the arcuate trend of the sill sheets. A zone dominated by strike-slip faulting in the north may be indicative of a lateral ramp geometry to the sill and would be consistent with left-lateral shear as the sill is emplaced. In the south, a change from contractional (~E–W shortening) to extensional (~N–S extension) appears coincident with the southern termination of the eastern body and, therefore, a change in the local boundary conditions.

Our observations and newly proposed emplacement model may have important implications for understanding how deformation structures accommodate the volumetric addition of magma in the subsurface. Field and microscale structural and kinematic data can be used to infer intrusion geometries (dm to km scale), which can then be used to fill the data gap between well, outcrop, and larger-scale geometries imaged on seismic-reflection profiles.

ACKNOWLEDGMENTS

The terrestrial laser scanning field work carried out in this paper was funded by the Geological Society of London's Elspeth Matthews Award for Fieldwork. Thanks to Midland Valley for providing an academic license for the use of Move™ and FieldMove™ software in this study. The authors would like to thank O. Galland and C. Magee for their highly constructive reviews and D. Fastovsky and M. Williams for the editorial handling of the manuscript. P.W. would also like to thank R. Wilson and S. Gunnell for their support and assistance during fieldwork.

REFERENCES CITED

Antonellini, M.A., and Cambray, F.W., 1992, Relations between sills intrusions and bedding-parallel extensional shear zones in the Mid-continent Rift System of the Lake Superior region: *Tectonophysics*, v. 212, p. 331–349, [https://doi.org/10.1016/0040-1951\(92\)90299-L](https://doi.org/10.1016/0040-1951(92)90299-L).

- Aydin, A., 1978, Small faults formed as deformation bands in sandstone: Pure and Applied Geophysics, v. 116, p. 913–930, <https://doi.org/10.1007/BF00876546>.
- Aydin, A., and Johnson, A.M., 1978, Development of faults as zones of deformation bands and as slip surfaces in sandstone: Pure and Applied Geophysics, v. 116, p. 931–942, <https://doi.org/10.1007/BF00876547>.
- Aydin, A., and Johnson, A.M., 1983, Analysis of faulting in porous sandstones: Journal of Structural Geology, v. 5, p. 19–31, [https://doi.org/10.1016/0191-8141\(83\)90004-4](https://doi.org/10.1016/0191-8141(83)90004-4).
- Bellian, J.A., Kerans, C., and Jennette, D.C., 2005, Digital outcrop models: Applications of terrestrial scanning lidar technology in stratigraphic modeling: Journal of Sedimentary Research, v. 75, no. 2, p. 166–176, <https://doi.org/10.2110/jsr.2005.013>.
- Buckley, S.J., Howell, J.A., Enge, H.D., and Kurz, T.H., 2008, Terrestrial laser scanning in geology: Data acquisition, processing and accuracy considerations: Journal of the Geological Society of London, v. 165, no. 3, p. 625–638, <https://doi.org/10.1144/0016-76492007-100>.
- Bump, A.P., and Davis, G.H., 2003, Late Cretaceous–early Tertiary Laramide deformation of the northern Colorado Plateau, Utah and Colorado: Journal of Structural Geology, v. 25, p. 421–440, [https://doi.org/10.1016/S0191-8141\(02\)00033-0](https://doi.org/10.1016/S0191-8141(02)00033-0).
- Coleman, D.S., Gray, W., and Glazner, A.F., 2004, Rethinking the emplacement and evolution of zoned plutons: Geochronologic evidence for incremental assembly of the Tuolumne Intrusive Suite: California Geology, v. 32, p. 433–436, <https://doi.org/10.1130/G20220.1>.
- Cruden, A.R., and McCaffrey, K.J.W., 2001, Growth of plutons by floor subsidence: Implications for rates of emplacement, intrusion spacing and melt-extraction mechanisms: Physics and Chemistry of the Earth. Part A: Solid Earth and Geodesy, v. 26, no. 4–5, p. 303–315, [https://doi.org/10.1016/S1464-1895\(01\)00060-6](https://doi.org/10.1016/S1464-1895(01)00060-6).
- Cruden, A.R., McCaffrey, K.J.W., and Bungler, A., 2018, Geometric scaling of tabular igneous intrusions: Implications for emplacement and growth, in Breitkreuz, C., and Rocchi, S., eds., Physical Geology of Shallow Magmatic Systems: Dykes, Sills and Laccoliths: Springer, Cham, p. 11–38, https://doi.org/10.1007/11157_2017_1000.
- Davis, G.H., 1978, Monocline fold pattern of the Colorado Plateau, in Matthews, V.I., ed., Laramide Folding Associated with Basement Block Faulting in the Western United States: Geological Society of America Memoir 151, p. 215–234, <https://doi.org/10.1130/MEM151-p215>.
- Davis, G.H., 1999, Structural geology of the Colorado Plateau region of southern Utah, with special emphasis on deformation bands: Geological Society of America Special Paper 342, 157 p., <https://doi.org/10.1130/0-8137-2342-6.1>.
- de Saint Blanquat, M., and Tikoff, B., 1997, Development of magmatic to solid-state fabrics during syntectonic emplacement of the Mono Creek granite, Sierra Nevada Batholith, California, in Bouchez, J.L., Hutton, D.H.W., and Stephens, W.E., eds., Granite: From Segregation of Melt to Emplacement Fabrics: Dordrecht, Springer, v. 8, p. 231–252, https://doi.org/10.1007/978-94-017-1717-5_15.
- de Saint-Blanquat, M., Habert, G., Horsman, E., Morgan, S., Tikoff, B., Launeau, P., and Gleizes, G., 2006, Mechanisms and duration of non-tectonically, assisted magma emplacement in the upper crust: Black Mesa pluton, Henry Mountains, Utah: Tectonophysics, v. 428, p. 1–31, <https://doi.org/10.1016/j.tecto.2006.07.014>.
- Engel, C.G., 1959, Igneous rocks and constituent hornblendes of the Henry Mountains, Utah: Geological Society of America Bulletin, v. 70, p. 951–980, [https://doi.org/10.1130/0016-7606\(1959\)70\[951:IRACHO\]2.0.CO;2](https://doi.org/10.1130/0016-7606(1959)70[951:IRACHO]2.0.CO;2).
- Fossen, H., Schultz, R.A., Shipton, Z.K., and Mair, K., 2007, Deformation bands in sandstone: A review: Journal of the Geological Society of London, v. 164, p. 755–769, <https://doi.org/10.1144/0016-76492006-036>.
- Galland, O., Planke, S., Neumann, E.-R., and Malthe-Sørensen, A., 2009, Experimental modelling of shallow magma emplacement: Application to saucer-shaped intrusions: Earth and Planetary Science Letters, v. 277, p. 373–383, <https://doi.org/10.1016/j.epsl.2008.11.003>.
- Galland, O., Holohan, E., van Wyk de Vries, B., and Burchardt, S., 2015, Laboratory modelling of volcano plumbing systems: A review, in Breitkreuz, C., and Rocchi, S., eds., Dykes, Sills and Laccoliths: Physical Geology of Shallow Magmatic Systems: Advances in Volcanology 2: Springer, p. 147–214, https://doi.org/10.1007/11157_2015_9.
- Gilbert, G.K., 1877, Geology of the Henry Mountains, Utah: U.S. Geographical and Geological Survey of the Rocky Mountain Region, 170 p., <https://doi.org/10.3133/70038096>.
- Gilbert, G.K., 1896, Laccoliths in southeastern Colorado: The Journal of Geology, v. 4, p. 816–825, <https://doi.org/10.1086/607618>.
- Habert, G., and de Saint-Blanquat, M., 2004, Rate of construction of the Black Mesa bysmalith, Henry Mountains, Utah, USA, in Breitkreuz, C., and Petford, N., eds., Physical Geology of High-Level Magmatic Systems: Geological Society of London Special Publication 234, p. 143–159.
- Haug, O.T., Galland, O., Souloumiac, P., Souche, A., Guldstrand, F., and Schmiedel, T., 2017, Inelastic damage as a mechanical precursor for the emplacement of saucer-shaped intrusions: Geology, v. 45, p. 1099–1102, <https://doi.org/10.1130/G39361.1>.
- Hintze, L.E., and Kowallis, B.J., 2009, A Field Guide to Utah's Rock: Geological History of Utah: Brigham Young University Geology Studies Special Publication 9, 225 p.
- Holdsworth, R.E., McErlean, M.A., and Strachan, R.A., 1999, The influence of country rock structural architecture during pluton emplacement: The Loch Loyal syenites, Scotland: Journal of the Geological Society of London, v. 156, p. 163–175, <https://doi.org/10.1144/gsjgs.156.1.0163>.
- Horsman, E., Tikoff, B., and Morgan, S., 2005, Emplacement related fabric in a sill and multiple sheets in the Maiden Creek sill, Henry Mountains, Utah: Journal of Structural Geology, v. 27, p. 1426–1444, <https://doi.org/10.1016/j.jsg.2005.03.003>.
- Horsman, E., Morgan, S., de Saint-Blanquat, M., Habert, G., Nugent, A., Hunter, R.A., and Tikoff, B., 2009, Emplacement and assembly of shallow intrusions from multiple magma pulses, Henry Mountains, Utah: Earth and Environmental Science Transactions of the Royal Society of Edinburgh, v. 100, p. 117–132, <https://doi.org/10.1017/S1755691009016089>.
- Hunt, C.B., 1953, Geology and Geography of the Henry Mountains Region, Utah: U.S. Geological Survey Professional Paper 228, 234 p., <https://doi.org/10.3133/pp228>.
- Hutton, D.H.W., and McErlean, M., 1991, Silurian and Early Devonian sinistral deformation of the Ratagain granite, Scotland: Constraints on the age of Caledonian movements on the Great Glen fault system: Journal of the Geological Society of London, v. 148, p. 1–4, <https://doi.org/10.1144/gsjgs.148.1.0001>.
- Hutton, D.H.W., Dempster, T.J., Brown, P.E., and Decker, S.D., 1990, A new mechanism of granite emplacement: Intrusion in active extensional shear zones: Nature, v. 343, p. 452–455, <https://doi.org/10.1038/343452a0>.
- Jackson, S.E., and Pollard, D.D., 1988, The laccolith-stock controversy: New results from the southern Henry Mountains, Utah: Geological Society of America Bulletin, v. 100, p. 117–139, [https://doi.org/10.1130/0016-7606\(1988\)100<0117:TLSCNR>2.3.CO;2](https://doi.org/10.1130/0016-7606(1988)100<0117:TLSCNR>2.3.CO;2).
- Johnson, A.M., and Pollard, D.D., 1973, Mechanics of growth of some laccolithic intrusion in the Henry Mountains, Utah, I: Field observations, Gilbert's model, physical properties and flow of the magma: Tectonophysics, v. 18, p. 261–309, [https://doi.org/10.1016/0040-1951\(73\)90050-4](https://doi.org/10.1016/0040-1951(73)90050-4).
- Jones, R.R., McCaffrey, K.J.W., Clegg, P., Wilson, R.W., Holliman, N.S., Holdsworth, R.E., Imber, J., and Waggott, S., 2009a, Integration of regional to outcrop digital data: 3D visualisation of multi-scale geological models: Computers & Geosciences, v. 35, no. 1, p. 4–18, <https://doi.org/10.1016/j.cageo.2007.09.007>.
- Jones, R.R., Kokkalis, S., and McCaffrey, K.J.W., 2009b, Quantitative analysis and visualization of nonplanar fault surfaces using terrestrial laser scanning (LIDAR)—The Arkitsa fault, central Greece, as a case study: Geosphere, v. 5, p. 465–482.
- Kavanagh, J.L., Menand, T., and Sparks, R.S.J., 2006, An experimental investigation of sill formation and propagation in layered elastic media: Earth and Planetary Science Letters, v. 245, p. 799–813, <https://doi.org/10.1016/j.epsl.2006.03.025>.
- Kavanagh, J.L., Boutelier, D., and Cruden, A.R., 2015, The mechanics of sill inception, propagation and growth: Experimental evidence for rapid reduction in magmatic overpressure: Earth and Planetary Science Letters, v. 421, p. 117–128, <https://doi.org/10.1016/j.epsl.2015.03.038>.
- Krantz, R.W., 1989, Orthorhombic fault patterns: The odd axis model and slip vector orientations: Tectonics, v. 8, p. 483–495, <https://doi.org/10.1029/TC008i003p0483>.
- Magee, C., Stevenson, C.T.E., O'Driscoll, B., and Petronis, M.S., 2012, Local and regional controls on the lateral emplacement of the Ben Hiant Dolerite intrusion, Ardnamurchan (NW Scotland): Journal of Structural Geology, v. 39, p. 66–82, <https://doi.org/10.1016/j.jsg.2012.03.005>.
- Magee, C., Jackson, C.A.-L., and Schofield, N., 2013, The influence of normal fault geometry on igneous sill emplacement and morphology: Geology, v. 41, p. 407–410, <https://doi.org/10.1130/G33824.1>.
- Magee, C., Jackson, C.A.-L., and Schofield, N., 2014, Diachronous sub-volcanic intrusion along deep-water margins: Insights from the Irish Rockall Basin: Basin Research, v. 26, p. 85–105, <https://doi.org/10.1111/bre.12044>.
- Magee, C., Muirhead, J., Schofield, N., Walker, R.J., Galland, O., Holford, S., Spacapan, J., Jackson, C.A.-L., and McCarthy, W., 2018, Structural signatures of igneous sheet intrusion propagation: Journal of Structural Geology, <https://doi.org/10.1016/j.jsg.2018.07.010>.
- Malthe-Sørensen, A., Planke, S., Svensen, H., and Jamtveit, B., 2004, Formation of saucer-shaped sills, in Breitkreuz, C., and Petford, N., eds., Physical Geology of High-Level Magmatic Systems: Geological Society of London Special Publication 324, p. 215–227.

- McCaffrey, K.J.W., 1992, Igneous emplacement in a transpressive shear zone: Ox Mountains igneous complex: *Journal of the Geological Society of London*, v. 149, p. 221–235, <https://doi.org/10.1144/gsjgs.149.2.0221>.
- McCaffrey, K.J.W., Jones, R.R., Holdsworth, R.E., Wilson, R.W., Clegg, P., Imber, J., Holliman, N., and Trinks, I., 2005, Unlocking the spatial dimension: Digital technologies and the future of geoscience fieldwork: *Journal of the Geological Society of London*, v. 162, p. 927–938, <https://doi.org/10.1144/0016-764905-017>.
- Menand, T., 2008, The mechanics and dynamics of sills in layered elastic rocks and their implications for growth of laccoliths and other igneous complexes: *Earth and Planetary Science Letters*, v. 267, p. 93–99, <https://doi.org/10.1016/j.epsl.2007.11.043>.
- Morgan, S., Stanik, A., Horsman, E., Tikoff, B., de Saint Blanquat, M., and Habert, G., 2008, Emplacement of multiple magma sheets and wall rock deformation: Trachyte Mesa intrusion, Henry Mountains, Utah: *Journal of Structural Geology*, v. 30, p. 491–512, <https://doi.org/10.1016/j.jsg.2008.01.005>.
- Nelson, S.T., and Davidson, J.P., 1993, Interactions between mantle-derived magmas and mafic crust, Henry Mountains, Utah: *Journal of Geophysical Research*, v. 98, p. 1837–1852, <https://doi.org/10.1029/92JB02689>.
- Nelson, S.T., Davidson, J.P., and Sullivan, K.R., 1992, New age determinations of central Colorado Plateau laccoliths, Utah: Recognizing disturbed K–Ar systematics and re-evaluating tectonomagmatic relationships: *Geological Society of America Bulletin*, v. 104, p. 1547–1560, [https://doi.org/10.1130/0016-7606\(1992\)104<1547:NADOC>2.3.CO;2](https://doi.org/10.1130/0016-7606(1992)104<1547:NADOC>2.3.CO;2).
- Neves, S.P., Vauchez, A., and Archanjo, C.J., 1996, Shear zone-controlled magma emplacement or magma-assisted nucleation of shear zones?: Insights from northeast Brazil: *Tectonophysics*, v. 262, p. 349–364, [https://doi.org/10.1016/0040-1951\(96\)00007-8](https://doi.org/10.1016/0040-1951(96)00007-8).
- Passchier, C.W., and Trouw, R.A.J., 2005, *Microtectonics* (second edition): Berlin/Heidelberg, Springer, 366 p., <https://doi.org/10.1007/3-540-29359-0>.
- Passchier, C.W., Zhang, J.S., and Konopasek, J., 2005, Geometric aspects of synkinematic granite intrusion into a ductile shear zone—An example from the Yunmengshan core complex, northern China, in Bruhn, D., and Burlini, L., eds., *High-Strain Zones: Structure and Physical Properties*: Geological Society of London Special Publication 245, p. 65–80, <https://doi.org/10.1144/GSL.SP.2005.245.01.04>.
- Petit, J.-P., 1987, Criteria for the sense of movement on fault surfaces in brittle rocks: *Journal of Structural Geology*, v. 9, p. 597–608, [https://doi.org/10.1016/0191-8141\(87\)90145-3](https://doi.org/10.1016/0191-8141(87)90145-3).
- Pollard, D.D., and Johnson, A.M., 1973, Mechanics of growth of some laccolithic intrusions in the Henry Mountains, Utah, II: Bending and failure of overburden layers and sill formation: *Tectonophysics*, v. 18, p. 311–354, [https://doi.org/10.1016/0040-1951\(73\)90051-6](https://doi.org/10.1016/0040-1951(73)90051-6).
- Pollard, D.D., Muller, O.H., and Dockstader, D.R., 1975, The form and growth of fingered sheet intrusions: *Geological Society of America Bulletin*, v. 86, p. 351–363, [https://doi.org/10.1130/0016-7606\(1975\)86<351:TFAGOF>2.0.CO;2](https://doi.org/10.1130/0016-7606(1975)86<351:TFAGOF>2.0.CO;2).
- Polteau, S., Mazzini, A., Galland, O., Planke, S., and Malthe-Sørensen, A., 2008, Saucer-shaped intrusions: Occurrences, emplacement and implications: *Earth and Planetary Science Letters*, v. 266, p. 195–204, <https://doi.org/10.1016/j.epsl.2007.11.015>.
- Reches, Z., 1987, Determination of the tectonic stress tensor from slip along faults that obey the Coulomb yield condition: *Tectonics*, v. 6, p. 849–861, <https://doi.org/10.1029/TC006i006p00849>.
- Schmiel, T., Galland, O., and Breitreuz, C., 2017, Dynamics of sill and laccolith emplacement in the brittle crust: Role of host-rock strength and deformation mode: Control of host on sills and laccoliths: *Journal of Geophysical Research. Solid Earth*, v. 122, p. 8860–8871, <https://doi.org/10.1002/2017JB014468>.
- Schofield, N.J., Brown, D.J., Magee, C., and Stevenson, C.T., 2012, Sill morphology and comparison of brittle and non-brittle emplacement mechanisms: *Journal of the Geological Society of London*, v. 169, p. 127–141, <https://doi.org/10.1144/0016-76492011-078>.
- Spacapan, J.B., Galland, O., Leanza, H.A., and Planke, S., 2016, Igneous sill and finger emplacement mechanism in shale-dominated formations: A field study at Cuesta del Chihuido, Neuquén Basin, Argentina: *Journal of the Geological Society of London*, v. 174, p. 422–433, <https://doi.org/10.1144/jgs2016-056>.
- Stevenson, C.T.E., Owens, W.H., and Hutton, D.H.W., 2007, Flow lobes in granite: The determination of magma flow direction in the Trawenagh Bay Granite, northwestern Ireland, using anisotropy of magnetic susceptibility: *Geological Society of America Bulletin*, v. 119, no. 11–12, p. 1368–1386, <https://doi.org/10.1130/B25970.1>.
- Thomson, K., and Hutton, D., 2004, Geometry and growth of sill complexes: Insights using 3D seismic from the North Rockall Trough: *Bulletin of Volcanology*, v. 66, p. 364–375, <https://doi.org/10.1007/s00445-003-0320-z>.
- Thomson, K., and Schofield, N., 2008, Lithological and structural controls on the emplacement and morphology of sills in sedimentary basins, in Thomson, K., and Petford, N., eds., *Structure and Emplacement of High-Level Magmatic Systems*: Geological Society of London Special Publication 302, p. 31–44, <https://doi.org/10.1144/SP302.3>.
- Westerman, D.S., Dini, A., Innocenti, F., and Rocchi, S., 2004, Rise and fall of a nested Christmas-tree laccolith complex, Elba Island, Italy, in Breitreuz, C., and Petford, N., eds., *Physical Geology of High-Level Magmatic Systems*: Geological Society of London Special Publication 234, p. 195–213, <https://doi.org/10.1144/GSL.SP.2004.234.01.12>.
- Wetmore, P.H., Connor, C.B., Kruse, S.E., Callihan, S., Pignotta, G., Stremtan, C., and Burke, A., 2009, Geometry of the Trachyte Mesa intrusion, Henry Mountains, Utah: Implications for the emplacement of small melt volumes into the upper crust: *Geochemistry, Geophysics, Geosystems*, v. 10, Q08006, <https://doi.org/10.1029/2009GC002469>.
- Wilson, P.I.R., 2015, Direct linking of host rock deformation structures to the emplacement, morphology and accommodation of high-level igneous intrusion: The Henry Mountains, Utah [Ph.D. thesis]: London, Kingston University, 323 p.
- Wilson, P.I.R., and McCaffrey, K.J.W., 2013, Intrusion space problem: Digital mapping and analysis of the Maiden Creek satellite intrusion, Henry Mountains Utah: *Geoscientist*, v. 23, no. 6, p. 16–19.
- Wilson, P.I.R., McCaffrey, K.J.W., Wilson, R.W., Jarvis, I., and Holdsworth, R.E., 2016, Deformation structures associated with the Trachyte Mesa intrusion, Henry Mountains, Utah: Implications for sill and laccolith emplacement mechanisms: *Journal of Structural Geology*, v. 87, p. 30–46, <https://doi.org/10.1016/j.jsg.2016.04.001>.